

筑波大学

博士 (医学) 学位論文

Antioxidant Nanomedicine with Cytoplasmic Distribution
in Neuronal Cells Shows Superior Neurovascular
Protection Properties for Ischemic Stroke in Mice

(神経細胞の細胞質に分布する

抗酸化剤ナノメディシンはマウスの虚血性脳卒中に
おいて優れた神経血管保護特性を示す)

2020

筑波大学大学院博士課程人間総合科学研究科

Arnela Mujagić

List of abbreviations

BBB	Blood brain barrier
CCA	Common carotid artery
DAPI	4',6-diamidino-2-phenylindole
EB	Evans blue
ECA	External carotid artery
ESR	Electron spin resonance
ICA	Internal carotid artery
IVT	Intravenous thrombolysis
HBSS	Hank's balanced salt solution
LMW	Low molecular weight
NP	Nanoparticles
NSS-R	Revised Neurobehavioral Severity Scale
PFA	Paraformaldehyde
PBS	Phosphate-buffered saline
ROS	Radical oxygen species
RNPs	Nitroxide conjugating nanoparticles
tMCAO	Transient middle cerebral artery occlusion

Table of Contents

CHAPTER 1 INTRODUCTION	5
1.1. Ischemic stroke and mechanical thrombectomy	
1.2. Ischemia-reperfusion injury and reactive oxygen species	
1.3. Nitroxide conjugating nanoparticles RNPs	
1.4. Treatment of the cerebral ischemia-reperfusion injury using RNPs	
CHAPTER 2 THE PURPOSE OF THE STUDY	10
CHAPTER 3 MATERIALS AND METHODS.....	11
3.1 Animals	
3.2 Drug preparation and administration	
3.3 The tMCAO model	
3.4 Evaluation of survival rate, neurological deficit and infarct size	
3.5 Evaluation of BBB disruption	
3.6 Distribution of Rhodamin-labelled RNPs in the infarct area	
3.7 Visualization of EB extravasation	
3.8 Evaluation of microglia polarization	
3.9 Evaluation of free radical scavenging capacities using electron spin resonance	
3.10 Evaluation of mitochondrial superoxide radical scavenging capacities	
3.11 Ethics	
3.12 Statistical analysis	
CHAPTER 4 RESULTS.....	22
4.1 Effects of RNPs and edaravone on survival rate and neurological deficit 24 h post-injection	
4.2 Effect of RNPs on BBB disruption	
4.3 Rhodamine-labeled RNPs distribution in the ischemic brain hemisphere 24 h post-injection	

4.4 Perivascular extravasation of EB	
4.5 Effects of RNPs on microglia polarization into M2 microglia	
4.6 Effects of RNPs on multiple ROS-scavenging capacities in the ischemic brain	
4.7 Effects of RNPs on mitochondrial superoxide scavenging capacities	
CHAPTER 5 DISCUSSION.....	27
5.1 Determination of the dose of RNPs	
5.2 RNPs and other nanoparticles	
5.3 Neuroprotective effects of RNPs	
5.4 Limitations and future challenges	
CHAPTER 6 CONCLUSION.....	32
CHAPTER 7 FIGURE LEGENDES.....	33
CHAPTER 8 FIGURES.....	37
CHAPTER 9 REFERENCES.....	59
CHAPTER 10 SOURCE	65
CHAPTER 11 ACKNOWLEDGMENTS.....	66

CHAPTER 1 INTRODUCTION

1.1 Ischemic stroke and mechanical thrombectomy

After ischemic heart disease, stroke is the second-most common cause of mortality and the third most common cause of disability worldwide. [1–9] Increased stroke burden over the past 25 years has been growing, especially in the developing countries, where the highest stroke DALYs (disability-adjusted life-years) and mortality rates have been reported. Stroke is one of the leading public health problems, because it is the main cause of physical and cognitive incapacities among the working population. Although stroke mortality has been in a decline globally since 1990s, the absolute number of people who died from stroke, remained disabled from stroke or survived stroke has increased. [1–9] Stroke is no longer a disease of the elderly, considering that according to the Global Burden of Disease Study of 2013, two-thirds of all strokes occur among people <70 years of age. Physical and intellectual limitations that lead to the high social cost of the stroke, develop in majority of the stroke survivors. [4]

Majority of all stroke cases are ischemic stroke due to cerebral artery occlusion, a life-threatening condition following neurological disorder. [5,6] Ischemic stroke is acute reduction in cerebral blood flow caused by in situ thrombosis or embolization of preexisting blood clot. Intravenous thrombolysis (IVT) by recombinant tissue plasminogen activator (rt-PA) has been used for the past 20 years as a treatment option for restoration of the blood flow in the occluded cerebral artery. However, IVT has to be administered within 4.5 hours of symptom onset and has many contraindications, such as active bleeding and present coagulation abnormalities. [5,6] IVT is not so effective in reestablishing blood flow in occluded large brain artery, and in the case of the middle cerebral artery blood flow was reestablished in 37.8% of the treated cases. [10] Taking in consideration that stroke on the basis of middle cerebral artery occlusion is especially disabling,

desirable clinical outcome of functional independence is difficult to obtain in majority of the treated patients. [10]

Mechanical thrombectomy using a stent retriever is an efficient and safe method of recanalizing of the emergent large vessel occlusion in the brain. With its establishment as therapy for an acute cerebral artery occlusion, treatment of severe ischemic stroke entered a new era. However, even if the occluded cerebral artery is recanalized by thrombectomy, the poor prognosis due to intracranial hemorrhage and expansion of cerebral infarction was described in 54%, and death in 15.3% of the patients in 2016 HERMES collaborators study. [2-9]

1.2. Ischemia-reperfusion injury and reactive oxygen species

Already damaged brain tissue gets additionally damaged after the recanalization, during reperfusion when reactive oxygen species (ROS) generation occurs; ROS impair survival and neurological function, causing secondary brain injury that can lead to hemorrhage in the ischemic area and brain edema. [11,12] In the ischemic brain, tissue damage occurs on the basis of excitotoxicity; rapid release of glutamate and its reuptake as a result of energy deprivation. This accumulation of glutamate activates a signal transduction system generating calcium influx that leads to an increase in intracellular calcium concentration. [11,12] Following, reactive oxygen species are generated in ischemic tissues due to activation of the signal transduction system involved in cyclooxygenase and nitric oxide synthesis. [11-14] Human ischemic brain is highly sensitive to oxidative damage because of its large oxygen consumption, large iron and unsaturated fatty acids contents, and a low intrinsic antioxidant effect. [11–14] Therefore, inhibiting oxidative

stress that occurs after reperfusion can reduce secondary brain damage, and result in improvement in prognosis of stroke patients.

Nitroxide radicals that can suppress oxidative stress are a potential therapeutic strategy because of their reported neuroprotective effects in rodent brain ischemia models. [11–14] 4-Hydroxy-2,2,6,6-tetramethylpiperidine-1-oxyl (TEMPOL) is a stable nitroxide radical compound with ability to suppress ROS acting as superoxide dismutase (SOD) and ability to inhibit a lipid peroxidation. TEMPOL can scavenge oxygen radicals by catalyzing redox transformation. [15,16] However, this low molecular weight (LMW) nitroxide radical showed several problems caused by its low molecular weight; it can penetrate through healthy brain tissue that was not affected by ischemia, and that leads to its short in vivo half-life. TEMPOL can induce hypotension by increasing nitric oxide in endothelial cells and there is a possibility that LMW radicals can penetrate into healthy cell mitochondria, interfere with normal redox reactions and cause serious side effects. [15,16]

1.3. Nitroxide conjugating nanoparticles RNPs

In order to solve these problems, Yukio Nagasaki from University of Tsukuba, designed and developed nitroxide conjugating nanoparticles, RNPs, by covalently bonding TEMPO to a highly bio-compatible block copolymer (redox polymer) and allowing it to self-assemble in an aqueous solution. [15,16,17] (Fig.1A) A redox-active nitroxide radical (4-amino-TEMPOL)-conjugating polymer (PEG-b-poly [4-(2,2,6,6-tetramethylpiperidine-1-oxyl) amino methyl styrene] [PEG-b-PMNT]) can self-assemble and form nanoparticles (NPs). These NPs are core-shell type nanoparticles, they have 30 nm diameter and 60 times longer half-life after intravenous injection compared with TEMPOL. NPs are pH sensitive, and core-centered amino group

protonation leads to a disintegration under acidic conditions, such as low pH in an ischemic brain tissue. [15,16,17] (Fig. 1B)

Previous studies have confirmed the positive effects of intra-arterial injection of nitroxide radical-conjugating nanoparticles (RNPs), after reperfusion, and obtained insight into the promising potential of RNPs in the treatment of stroke, following mechanical thrombectomy. [15,16,17] Intravenous injection of RNPs in a dose of 90 mg/kg has neuroprotective effects against cerebral ischemia-reperfusion injury in a rat middle cerebral artery occlusion model. [16] Intra-arterial injection of RNPs in a dose of 9 mg/kg inhibits blood-brain barrier (BBB) disruption in the ischemic area, improves neurological deficit, decreases the infarct volume, and improves the ROS-scavenging capacity in a mouse transient middle cerebral artery occlusion (tMCAO) model. [15] RNPs demonstrated neuroprotective effect in a traumatic brain injury mouse model, by significantly improving the radical oxygen species scavenging activity and supporting polarization of microglia cells into neuroprotective microglia M2 cells. [28]

However, the effects of RNPs and other conventional ROS scavengers have not been compared, and the RNP distribution is still unclear.

1.4. Treatment of the cerebral ischemia-reperfusion injury using RNPs

This study investigated whether RNPs can be a promising antioxidant and neuroprotective nanomedicine for the treatment of cerebral ischemia-reperfusion injury after mechanical thrombectomy in acute ischemic stroke. We compared the neuroprotective effects of RNPs and edaravone (Radicut®), a „free-radical scavenger that was marketed in Japan by Mitsubishi Tanabe Pharma Corporation in 2010 as the treatment for acute ischemic stroke”. [18]

Edaravone is a low molecular weight lipophilic free radical scavenger that can cross blood-brain-barrier. In a previously published rodent stroke study, edaravone did not show any behavioral improvement or cell survival. However, it was able to attenuate polyvinyl acetate changes in brain monoamine metabolism. [18-22] Standard ischemia model in gerbils study showed that although edaravone increased cerebral blood flow and reduced brain edema, it had no effect on neuronal survival or mortality rate compared to control group. [18-22] Edaravone pre-treatment in the dose of 3mg/kg i.v. prolonged survival time in rat subjected to global ischemia and reduced BBB dysfunction while post-treatment decreased cortical infarct size. [18-22]

In this study, we evaluated the RNPs distribution in the ischemic brain and compared the effects of intra-arterially injected RNPs and edaravone on survival rate, neurological deficit, and BBB damage that follow cerebral ischemia-reperfusion injury in mice. Next, we determined the cerebral ROS-scavenging capacity of RNPs and edaravone; and mitochondria generated oxygen radical scavenging capacity. Finally, by analyzing the RNPs presence and distribution around endothelial cells, neurons, astrocytes, and microglia, we studied neurovascular unit protection.

CHAPTER 2 THE PURPOSE OF THE STUDY

The purpose of this study is the development of antioxidant nanomedicine RNPs as the new brain protective drug and elucidation of its neuroprotective mechanism using a mouse cerebral ischemia-reperfusion injury model, tMCAO model.

To accomplish this, we compared the neuroprotective effects of RNPs and edaravone, free-radical scavenger that is in use in Japan. By examining the neuroprotective effect of RNPs on a neuro-vascular unit in the peri-infarction area, and RNPs ROS scavenging capacities after the ischemia-reperfusion, we have confirmed the superiority of RNPs when compared to edaravone, medicine marketed in Japan.

CHAPTER 3 MATERIALS AND METHODS

3.1 Animals

Male C57BL/6J mice (age 6–7 weeks; body weight 20–25 g) were purchased from Charles River Laboratories Japan, Inc. Experiments have been reported in compliance with ARRIVE guidelines.

3.2 Drug preparation and administration

pH-sensitive RNPs were prepared from a poly(ethylene glycol)-*b*-poly(methylstyrene) (PEG-*b*-PMS) block copolymer, covalently conjugated to 4-amino-2,2,6,6-tetramethylpiperidine-*N*-oxyl (amino-TEMPOL) (PEG-*b*-PMNT), as previously described. [15,23,24] By dialysis, PEG-*b*-PMNT formed a core-shell self-assembling polymeric micelle in aqueous media. [15,23,24] The average RNP diameter and zeta potential were 33 ± 6 nm and -0.15 mV, respectively, measured using a Zetasizer Nano light-scattering spectrometer (Malvern Instruments, Malvern, USA). [15,23,24]

Prior to this study, dose-dependent RNPs and edaravone efficiency pilot studies were conducted to determine the most appropriate dose of these two medicines for intra-arterial injection. The survival rate and neurological deficit were evaluated after intra-arterial injections of 0.09 mg/kg, 0.9 mg/kg, and 9 mg/kg ($n = 6$ each) of RNPs and 0.03 mg/kg, 0.3 mg/kg, and 3 mg/kg ($n = 6$ each) of edaravone. The control group was given PBS ($n = 6$), and 24 h post-injection, the mice were euthanized. Based on the survival rate, we decided to use 9 mg/kg of RNPs and 3 mg/kg of edaravone (Fig. 2).

3.3 The tMCAO model

The tMCAO model was made as previously described in the Koizumi method. [25] The mice were anesthetized using through intraperitoneal injection: 70 mg/kg ketamine and 16 mg/kg xylazine. The right common carotid artery (CCA), internal carotid artery (ICA), and external carotid artery (ECA) were presented and the ECA and proximal CCA ligated under an operating microscope. After a small arteriotomy at the CCA, 6-0 nylon suture with silicon coating (6021 PK5Re; Docol Corporation, Sharon, MA, USA) was inserted into the ICA through the CCA, all the way to the origin of the middle cerebral artery. The filament measurements were as follows: size, 6-0; diameter, 0.09–0.11 mm; length, 20 mm; diameter with coating, 0.21 ± 0.02 mm; and coating length, 1.5–2 mm.

After 60 min of occlusion and after carefully removing the 6-0 nylon suture, reperfusion was allowed for 20 min. During surgery and recovery, the body temperature was maintained at 37°C using a heating pad. After 20 min of reperfusion, we examined the neurological deficit and randomly divided the mice into groups: intra-arterial RNPs injection (RNP group), intra-arterial edaravone injection (edaravone group), and PBS group (control group).

Next, the RNP group was administered RNP (7 μ M/kg, 9 mg/kg, 1 mg/mL solution) into the right CCA using a PE10 polyethylene tube. Similarly, the edaravone and control groups were administered edaravone (17 μ M/kg, 3 mg/kg) and PBS, respectively. The mice were left to recover for 24 h and provided soft food and water in a room with controlled temperature, humidity, and light exposure. Then, 24 h after intra-arterial injection of RNPs, edaravone, or PBS, neurological deficit was again examined. Finally, the mice were euthanized using intraperitoneal injection of 40 mg/kg of pentobarbital sodium (Somnopentyl®, Kyoritsu Seiyaku). (Fig. 3)

3.4 Evaluation of survival rate, neurological deficit, and infarct size

To evaluate the neurological deficit after tMCAO and 24 h post-injection of medicines, we used two different scales and the rotarod test. Scales used in this study are modified Longa score and The Revised Neurobehavioral Severity Scale (NSS-R).

Modified Longa score consists out of seven points, given as follows: 0, no neurological deficit; 1, failure to extend right forepaw; 2, decreased grip of right forelimb while tail gently pulled; 3, contralateral circling only if pulled by tail; 4, circling or walking to the right; 5, walking only if stimulated; 6, unresponsive to stimulation; and 7, dead. Mice with a Longa score of 3, 4, or 5 were used for further analysis because they had obvious signs of infarction but were still able to move in the cage and eat by themselves. These mice were evaluated again for neurological deficit and then euthanized. Based on the results of a previously conducted pilot study and power analysis, 20 animals per group was determined to be sufficient to evaluate survival rate, neurological deficits, and infarct area size. Total of 69 mice underwent tMCAO. The RNP and edaravone groups comprised 20 mice each and control group had 12 mice. Seventeen mice had Longa score 1, 2, 6, or 7 after tMCAO and were not used for further analysis. These mice were euthanized. The survival rate was presented as a percentage of surviving mice in a group.

After transcardiac perfusion with PBS, the mice's brains were removed, fixated overnight in 4% paraformaldehyde (PFA), dehydrated in 30% sucrose for 48 h, frozen above liquid nitrogen embedded in Tissue-Tek O.C.T compound (Sakura Finetek Japan), and stored at -80°C for further use. Using a cryostat, 10 μm frozen coronal brain sections were cut, fixed in 4% PFA, and stained with Cresyl violet. Mice that died during 24 h post-injection were not included for evaluation of infarct size. As previously described, infarct size was calculated as the ratio of the total infarct area

using five coronal sections (starting 2 mm anterior to the bregma, every 1 mm section) to the area in the contralateral hemisphere and presented as a percentage. [15]

The second scale that we used to evaluate neurological deficit 24 h post-injection of medicines, was previously described by Yarnell et al. [26] The Revised Neurobehavioral Severity Scale evaluates not only balance and motor coordination, but also motor and sensory reflexes in mice. Tasks are performed in precise order that is „designed to minimize any “contamination” or interference of one task with the other“. [26] Tasks are as follows: behavioral evaluation of balance, landing, tail raise, dragging, righting reflex, ear reflex, eye reflex, sound reflex, tail pinch, and hindpaw pinch. All tasks are scored using three point Likert scale. Normal, healthy response is scored as 0, partial or compromised response as 1 and the absence of a response as 2. Mice that died during 24 h post-injection of medicine were not evaluated using NSS-R. Total of 14 mice underwent tMCAO. The RNP, edaravone and control groups comprised 4 mice each. Two mice died during the recovery period after tMCAO and were not included in further analysis.

To evaluate sensorimotor coordination and motor learning 24 h after tMCAO, we used rotarod test. Test is performed in a way that mouse is placed on a rotarod device and time taken for the mouse to fall off was recorded. [27,28] Each mouse was trained on the rotarod device for 2 days before the tMCAO, 3 times per day with 1 hour rest periods in between. At the end of training, mice were evaluated and the base line values were recorded. In this study we used single lane rotarod (MK-630B, Muromachi Kikai Corporation, Japan). Initial speed of rotor was 4 rpm and was gradually increased to 40 rpm in 5 minutes. Total of 12 mice underwent tMCAO. The RNP, edaravone and control groups comprised 4 mice each. 24 h post-injection of medicine mice were evaluated 3 times and the average time taken for mouse to fall was recorded.

3.5 Evaluation of BBB disruption

To evaluate BBB disruption that follows tMCAO-induced injury, we used two different methods. First one was Evans Blue extravasation assay. 2% EB solution in PBS (4 mL/kg) was intraperitoneally injected 30 min after RNPs ($n = 6$) or edaravone ($n = 6$) was injected. [15,29] Neurological examination was performed after tMCAO and 24 h post-injection of RNPs or edaravone. To remove the intravascular EB, intracardiac perfusion with PBS was performed before euthanization. Mice were euthanized 24 h post-injection of EB. The ischemic brain hemisphere was removed, homogenized in 1 mL of 50% trichloroacetic acid solution, and centrifuged. The absorbance of the supernatant was measured at a wavelength of 620 nm using a Mithras LB 940 spectrophotometer (Berthold Technologies GmbH & Co. KG, Germany) [15,29] and quantified according to a standard curve. The results were presented as μg of EB stain/g of ischemic brain hemisphere.

Second method, that we used to evaluate BBB disruption, was BBB permeability assay using FITC dextran 4kD. [21] One hundred μL of 2 mM FITC dextran 4kD solution was injected intraperitoneally 24 h after the injection of RNPs, edaravone or PBS ($n = 4$ each). Fifteen minutes after FITC dextran injection, mice were sacrificed by an intraperitoneal injection of pentobarbital (40 mg/kg) and 200 μL of blood sample was collected from the right atrium. To remove intravascular FITC dextran intracardiac perfusion with fresh, cold PBS was performed through the left ventricle. Mice were euthanized and ischemic brain hemisphere was removed, weighed and homogenized it in 200 μL of PBS. Brain homogenates and blood samples were centrifuged and fluorescence of the supernatant and blood serum were measured at 490/520 nm with a spectrophotometer (Mithras LB 940, BERTHOLD technologies GmbH & Co. KG). Quantification was done after subtracting sham animal values. The results are presented as raw fluorescence units

RFUs. Permeability index was calculated using following formula: Permeability Index (mL/g) = (Tissue RFUs/g tissue weight)/ (Serum RFUs/mL serum). [30]

3.6 Distribution of Rhodamine-labeled RNPs in the infarct area

To evaluate the RNPs presence and distribution in the ischemic brain, we used rhodamine-labeled RNPs (Rh-RNPs). Rh-RNPs was prepared as previously described. Before performing dialysis from dimethylformamide (DMF) solution against water, we added rhodamine-*N*-hydroxysuccinimide to the DMF solution of PEG-*b*-PMNT block copolymer. Process was followed by dialysis against water. [15]

After 60 min of occlusion and 20 min of reperfusion, Rh-RNPs were intra-arterially injected, and the mice were euthanized 24 h post-injection of RNPs ($n = 4$). Frozen coronal brain sections were fixed in 4% PFA, washed twice in PBS, and incubated with primary antibodies diluted in PBS containing 1% bovine serum albumin overnight at 4°C.

The following primary antibodies were used: rat polyclonal anti-mouse CD31 (1:100 dilution; #550274; BD Biosciences, San Jose, CA, USA) and mouse monoclonal Anti-rhodamine (1:250 dilution; ab9093; Abcam, Cambridge, UK) to visualize RNPs distribution around endothelial cells; rabbit monoclonal anti-NeuN (1:500 dilution; ab9093; Abcam) and mouse monoclonal Anti-rhodamine (1:250 dilution; ab9093; Abcam) to visualize RNPs distribution around neuronal cells; rabbit polyclonal anti-glial fibrillary acidic protein (anti-GFAP; 1:500 dilution; ab7260; Abcam) and mouse monoclonal Anti-rhodamine (1:250 dilution; ab9093; Abcam) to visualize RNPs distribution around astrocytes; rabbit polyclonal anti-iba-1 (1:500

dilution; 019-19741, Wako Chemicals, Richmond, VA, USA) and mouse monoclonal Anti-rhodamine (1:250 dilution; ab9093; Abcam) to visualize RNPs distribution around microglia.

After primary antibody incubation, frozen coronal brain sections were washed twice with PBS and incubated with Alexa Fluor-conjugated secondary antibodies (1:400 dilution; Invitrogen, Carlsbad, CA, USA) for 60 min at room temperature. Cell nuclei were visualized using a mounting medium with 4',6-diamidino-2-phenylindole (DAPI; #SCR-38448; Dianova GmbH, Germany). Brain slides were observed under a Biozero BS8000 fluorescent microscope (Keyence Corporation of America, Itasca, IL, USA). Frozen brain sections from PBS-treated mice that were stained using the same protocol were observed as negative control.

The same protocol was used on 50 μm thick coronal frozen sections obtained from mice administered RNP ($n = 4$) to evaluate RNPs distribution in and around NeuN-positive neuronal cells using a Leica TCS SPE laser scanning confocal microscope (Leica Microsystems, Wetzlar, Germany).

3.7 Visualization of EB extravasation

To visualize EB extravasation around CD31-positive endothelial cells, we used the previously described protocol on 10 μm frozen brain coronal sections obtained by euthanizing mice 24 h post-injection of EB. Briefly, EB was intraperitoneally injected into mice 30 min post-injection of RNPs and edaravone ($n = 4$ each), but no primary antibody was used. [31]

3.8 Evaluation of microglia polarization

We evaluated the effects of RNPs and edaravone on microglia polarization into neurotoxic microglia M1 and neuroprotective microglia M2 using mice intra-arterially injected with RNPs, edaravone, or PBS ($n = 4$ each). We used the following primary antibodies: rabbit polyclonal anti-iba-1 (1:500 dilution; 019-19741, Wako Chemicals), purified rat anti-CD16/32 (1:500 dilution; 553142, BD-Pharmigen), and mouse monoclonal Anti-rhodamine (1:250 dilution; ab9093; Abcam) to visualize microglia M1; rabbit polyclonal anti-iba-1 (1:500 dilution; 019-19741, Wako Chemicals), goat polyclonal anti-CD206 (1:500 dilution; AF2535, R&D Systems, Minneapolis, MN, USA) and mouse monoclonal Anti-rhodamine (1:250 dilution; ab9093; Abcam) to visualize microglia M2.

Mouse monoclonal Anti-rhodamine was not used in the edaravone group. Frozen brain sections from PBS-treated mice that were stained using the same protocol were observed as negative control.

The sum of iba-1-CD16/32 and iba-1-CD206 double-positive cells was calculated for three consecutive brain sections ($\times 400$) in three randomly selected places in the peri-infarction area. Results were presented as cells/mm².

3.9 Evaluation of free-radical-scavenging capacities using electron spin resonance

We measured multiple free-radical-scavenging (MULTIS) capacities in ischemic brains using electron spin resonance (ESR). [15,32] The scavenging capacities of four free radicals were measured: superoxide (O_2^-), hydroxyl ($\cdot OH$), alkoxy ($RO\cdot$), and alkyl peroxy ($ROO\cdot$) radicals.

The mice were euthanized 24 h post-injection of RNPs and edaravone ($n = 4$ each). PBS perfusion was done through the left ventricle, and ischemic brain hemispheres were removed and homogenized in 700 μL of PBS, as previously described. [15] After centrifuging, supernatants were collected and stored at $-80^\circ C$ until further use. Free radicals were obtained via *in situ* irradiation with ultraviolet-visible (UV-visible) light using an RUVF-203SR UV illuminator (Radical Research Inc., Tokyo, Japan). The ESR spin-trapping reagent used was 5-(2,2-dimethyl-1,3-propoxycyclophosphoryl)-5-methyl-1-pyrroline-*N*-oxide (CYPMPO; RR Inc, Tokyo, Japan). [15] Dissolved in phosphate buffer free-radical precursors or sensitizers and supernatants of brain homogenates (1.7–3.4 vol.%) were added to the reaction mixtures. [15] The RRX-1X ESR spectrometer equipped with WIN-RAD operation software (Radical Research Inc.) was used.

ROS-scavenging activity was calculated as unit equivalents to known pure scavengers for each ROS: Glutathione (GSH) for $\cdot OH$, Superoxide dismutase (SOD) for O_2^- , 6-Hydroxy-2,5,7,8-tetramethylchroman-2-carboxylic acid (TROLOX) for $RO\cdot$, A-lipoic acid (α -LA) for $ROO\cdot$. [15].

3.10. Evaluation of mitochondrial superoxide radical-scavenging capacities

We measured fluorescence intensity of the cells in the peri-infarction area and the core of the infarction area and evaluated the scavenging effects of RNPs and edaravone on mitochondria generated superoxide radical.

After 60 min of occlusion and 20 min of reperfusion, RNPs, edaravone and PBS, respectively, were intra-arterially injected, and the mice were euthanized 24 h post-injection ($n = 4$ each). Frozen coronal brain sections were fixed in 4% PFA, washed twice in Hank's balanced salt solution (HBSS) and incubated with mitochondrial probes diluted in HBSS for 15 minutes at 4°C. Following mitochondrial probes were used: MitoSOX™ Red mitochondrial superoxide indicator (0.1 μM dilution, M36008, Molecular Probes™, Invitrogen detection technologies) to detect superoxide in the mitochondria; and MitoTracker® Green FM (20 nM dilution, M7514, Molecular Probes™, Invitrogen detection technologies) to label mitochondria. After 15 minutes of incubation brain sections were washed in HBSS twice and cell nuclei were visualized using a mounting medium with 4',6-diamidino-2-phenylindole (DAPI; #SCR-38448; Dianova GmbH, Germany). Brain slides were observed under a Biozero BS8000 fluorescent microscope (Keyence Corporation of America, Itasca, IL, USA). PBS-treated mice frozen brain sections were observed as negative control. Cell fluorescence was measured using ImageJ.

To evaluate the mitochondrial superoxide radical scavenging activity we measured the fluorescence of MitoSOX™ Red positive cells in three randomly selected places in the peri-infarction area and in the core of the infarction area; in a 3 consecutive brain sections (×1000). Results were presented as an average corrected total cell fluorescence.

3.11 Ethics

All animal experiments were approved by the Animal Experiment Committee of the University of Tsukuba, Ibaraki, Japan (approval no. 18-106). The experiments were performed according to the *Guide for the Care and Use of Laboratory Animals* (www.nap.edu).

3.12 Statistical analysis

Statistical analysis was performed using SPSS Statistics (IBM Corporation, Japan). Parametric data were compared using Student's *t*-test and analysis of variance, whereas nonparametric data were compared using the Mann-Whitney *U* test and the Kruskal-Wallis test. Calculated values were expressed as means \pm standard deviation. $P \leq 0.05$ was considered statistically significant.

CHAPTER 4 RESULTS

4.1 Effects of RNPs and edaravone on survival rate and neurological deficit 24 h post-injection

RNPs significantly improved the survival rate compared with edaravone and control group. In the RNP group, 14 of 20 mice (70%) survived compared with 8 of 20 mice (40%) in the edaravone group ($P < 0.05$) and 4 of 12 mice (33.33%) in the control group ($P < 0.05$) 24 h post-injection (Fig. 4A). RNPs significantly improved neurological deficit 24 h post-injection. The neurological deficit Longa score was 4.85 ± 1.63 in the RNP group compared with 6.05 ± 1.32 in the edaravone group ($P < 0.05$) and 6.5 ± 0.78 in the control group ($P < 0.05$) (Fig. 4B). The infarct size, calculated using mice that survived 24 h post-injection, was $29.16\% \pm 6.25\%$ in the RNP group ($n = 14$) versus $32.76\% \pm 2.80\%$ in the edaravone group ($n = 8$) ($P = 0.10$). RNPs significantly improved neurological deficit 24 h post-injection measured using The Revised Neurobehavioral Severity Scale (NSS-R). Although analysis of variance did not show significant difference between three compared groups ($P = 0.10$), post hoc analysis showed significant difference between RNP group and edaravone group; and RNP and control group. The NSS-R score was 6.75 ± 0.96 in the RNP group ($n = 4$) compared with 12.25 ± 2.5 in the edaravone group ($n = 4$) ($P < 0.05$) and 12.25 ± 2.99 in the control group ($n = 4$) ($P < 0.05$) (Fig. 4C). RNPs significantly improved sensorimotor coordination and motor learning 24 h post-injection measured in seconds using rotarod test. RNP group animals took longer to fall of the rotarod device compared to edaravone and control group ($P = 0.05$). The time that took animals to fall of the device was 99 ± 33.54 s in the RNP group ($n = 4$) compared with 41.25 ± 13.89 s in the edaravone group ($n = 4$) ($P < 0.05$) and 40 ± 4.76 s in the control group ($n = 4$) ($P < 0.05$) (Fig. 4D).

4.2 Effect of RNPs on BBB disruption

RNPs significantly inhibited Evans blue (EB) extravasation compared with edaravone (Fig. 5A). EB leakage, expressed as $\mu\text{g/g}$ of ischemic brain hemisphere, was 15.84 ± 8.47 in the RNP group ($n = 4$) versus 37.05 ± 12.88 in the edaravone group ($n = 4$) ($P < 0.05$) (Fig. 5B).

RNPs significantly inhibited BBB disruption and reduced BBB permeability 24 h post-injection. Although analysis of variance did not show significant difference between groups ($P = 0.28$), post hoc analysis showed significant difference between RNP group and edaravone group; and RNPs and control group. Brain permeability index expressed as 10^{-3} mL/g of ischemic brain hemisphere, was 0.017 ± 0.022 in the RNP group ($n = 4$) compared to 0.071 ± 0.053 in the edaravone group ($n = 4$) ($P < 0.05$) and 0.168 ± 0.119 in the control group ($n = 4$) ($P < 0.05$) (Fig. 5C).

4.3 Rhodamine-labeled RNPs distribution in the ischemic brain hemisphere 24 h post-injection

RNPs were detected by immunofluorescence analysis using Anti-rhodamine antibody and were localized in the endothelial cells, the perivascular space, neuronal cell cytoplasm, astrocytes, and microglia (Fig. 6). In this stage of Rh-RNPs distribution evaluation, we found a significant number of neuronal cells stained both with NeuN and Anti-rhodamine, indicating the possible presence of RNPs in their cytoplasm. Using confocal microscopy, we confirmed Rh-RNPs internalization and investigated whether we could find it in the nuclei. In real-time and three dimensions, we found Rh-RNPs in the perivascular space and in the cytoplasm of NeuN-positive cells but not in the nuclei of these cells (Fig. 7B). Using 3D reconstruction ($\times 1000$), we confirmed

our finding of Rh-RNPs in the perivascular space and in the cytoplasm of neuronal cells (Fig. 7C). These findings indicated that RNPs can cross the damaged BBB and accumulate not only in the extravascular ischemic area but also in the cytoplasm of neuronal cells. Anti-rhodamine antibody was not detected in the control samples (Fig. 8).

4.4 Perivascular extravasation of EB

Without using a primary antibody, we confirmed perivascular extravasation of EB that penetrated the damaged BBB and accumulated around CD31-positive cells. In the peri-infarction area, EB extravasation was localized in and around brain blood vessels and significantly higher in the edaravone group (Fig. 9).

4.5 Effects of RNPs on microglia polarization into M2 microglia

We confirmed the presence and polarization of microglia into neurotoxic microglia M1 and neuroprotective microglia M2 in the peri-infarction area 24 h post-injection of phosphate-buffered saline (PBS) (control group), RNP, and edaravone (Fig. 10). In the PBS group ($n = 4$), the number of microglia M1 cells was 302 ± 30.03 cells/mm², whereas that of microglia M2 cells was 39 ± 4.11 cells/mm². There was a significant difference in the number of microglia M2 cells between RNP and control groups ($P < 0.05$), but there was no significant difference in the number of microglia M1 cells between these groups ($P = 0.42$) (Fig.11).

The number of M1 cells was 230 ± 28.55 cells/mm² in the RNP group ($n = 4$) and 174 ± 15.15 cells/mm² in the edaravone group ($n = 4$). The number of M2 cells was 198 ± 25.25

cells/mm² in the RNP group ($n = 4$) and 68 ± 19.49 cells/mm² in the edaravone group ($n = 4$). We found a significant difference in the number of microglia M2 cells between RNP and edaravone groups ($P < 0.05$) but no significant difference in the number of microglia M1 cells between these groups ($P = 0.21$). These results indicated that RNPs can support the polarization of microglia into neuroprotective microglia M2, which are responsible for phagocytosis, inhibition of the inflammatory response, and tissue remodeling, repair, and healing.

4.6 Effects of RNPs on multiple ROS-scavenging capacities in the ischemic brain

Using the MULTIS capacity method, we evaluated the ROS-scavenging capacities in brain homogenates of RNP and edaravone groups (Fig. 12). The scavenging capacities of $\cdot\text{OH}$, $\text{RO}\cdot$, and ROO were significantly higher in the RNP group than in the edaravone group ($P < 0.05$), whereas the scavenging capacity of $\text{O}_2^{\cdot-}$ was not different between the groups ($P = 0.27$): for OH : Edaravone group, 3.38 ± 0.62 vs. RNP group 4.27 ± 0.23 mM-GSHeq; for RO : Edaravone group 55.56 ± 21.25 vs. RNP group 86.51 ± 11.96 mM-TROLOXeq; for ROO: Edaravone group 1336.57 ± 431.51 vs. RNP group 2809.63 ± 639.38 μM - α -LAeq and for $\text{O}_2^{\cdot-}$: Edaravone group 0.25 ± 0.076 vs. RNP group 0.33 ± 0.11 U/mL-SODEq.

4.7 Effects of RNPs on mitochondrial superoxide scavenging capacities

We evaluated mitochondrial superoxide radical scavenging activity by measuring the fluorescence of MitoSOX™ Red positive cells in the in the peri-infarction area and the core of the infarction area (Fig. 13, 14).

Average corrected total cell fluorescence in core of the infarction area was was 799163.87 ± 148081.28 for the RNP group ($n = 4$), 849880.04 ± 319378.11 for the edaravone group ($n = 4$) and 1149065.97 ± 247118.96 for the control group ($n = 4$) ($P = 0.15$) (Fig.13A). Average corrected total cell fluorescence in the peri-infarction area was 706322.75 ± 103122.48 for the RNP group ($n = 4$), 964479.81 ± 115661.39 for the edaravone group ($n = 4$) and 1123226.74 ± 185859.67 for the control group ($n = 4$) ($P < 0.05$) (Fig.13B). These results indicate that RNPs are powerful mitochondrial superoxide radical scavenger able to suppress destructive effect of the superoxide radical in the peri-infarction area of the ischemic brain.

CHAPTER 5 DISCUSSION

5.1. Determination of the dose of RNPs

Previous studies have confirmed the positive effect of intra-arterial RNPs injection after reperfusion in rodent tMCAO models. [15,16] In this study we evaluated the neuroprotective effect of RNPs by comparing it to the edaravone (Radicut®), free radical scavenger clinically used in Japan. To avoid the first-pass effect, intra-arterial administration is selected, which allows direct administration of medicines to the brain immediately after reperfusion. Prior pilot study confirmed the effectiveness of RNP in the dose of 9 mg/kg (7 μ M/kg) that is a 1/100 part of LD₅₀, and edaravone in the dose of 3 mg/kg (17 μ M/kg) that gave the best survival rate among the given groups. (Fig. 2)

5.2. RNPs and other nanoparticles

NPs that have densely packed PEG chain surfaces, such as RNPs, are retained better in blood circulation because of decreased clearance through the reticuloendothelial system. [15] This prolonged circulation time makes RNPs more efficient. The in vivo half-life of RNPs is 60 min, which is significantly longer than that of TEMPOL. [16] As most of the cell surfaces have slight negative charge, NPs with a positive charge are easily adsorbed onto the surface of tissues, making it difficult for NPs to circulate. In contrast, negatively charged NPs are taken up by scavenger receptors. [33] The surface of RNPs is not only PEGylated but also neutrally charged. Because of the densely packed PEG surface, small size and neutral surface charge, the dispersion stability of RNPs is much higher than that of conventional nanoparticles, which might improve permeability to neural sites via damaged BBB. Edaravone is present in a form of negatively charged anion and electrons released from the edaravone anion can scavenge radical species containing free electron.

[18] In theory, it is possible that negative charge can make an edaravone a target for scavenger receptors, and edaravone low molecular weight, can allow edaravone to penetrate into healthy cell mitochondria and interfere with normal redox reactions. Therefore, interactions between edaravone and scavenger receptors, and edaravone and normal redox reactions should be additionally investigated in the future in order to develop edaravone into the medicine that can be used worldwide. Rapid blood clearance of low-molecular-weight antioxidants, such as TEMPOL and edaravone, might not well internalize in neural sites even via damaged BBB as compared with the long-circulating RNPs. [15,16] When compared with TEMPOL, RNPs do not have serious side effects of low-molecular-weight radicals, such as hypotension. [16]

The diameter of RNPs is ~30 nm, making it smaller than other NPs. [34] Larger NPs have difficulty crossing the BBB, can interfere with serum proteins, and are needed in large amounts, which can cause cytotoxicity. As BBB permeability increases after reperfusion, small nanoparticles such as RNPs cross the BBB and have better access to ischemic brain tissue.

5.3. Neuroprotective effects of RNPs

Comparing the EB extravasation in the ischemic brain hemispheres between edaravone and RNP groups, intra-arterial RNPs injection significantly decreased EB extravasation, meaning better inhibition of BBB disruption during reperfusion. (Fig. 5) RNPs were also able to significantly inhibit BBB disruption by reducing BBB permeability 24 h post injection compared to edaravone. The reasons for these positive outcomes could be RNPs distribution in endothelial cells, which protects and supports the integrity of brain blood vessels from the oxidative damages. Increased BBB permeability that follows transient cerebral ischemia allows RNPs to enter brain

tissue and protect not only neuronal cells but also the BBB from reperfusion-caused damage. Previous studies [35-37] have followed microglia polarization from day 1 to day 14, unlike this study where we showed the first stages of microglia polarization 24 h after tMCAO and injection of medicines. (Fig.10) Compared to edaravone, RNPs can provide better conditions for microglia to polarize into microglia M2. These findings are suggesting that increased BBB permeability following transient cerebral ischemia allows RNPs not only to enter brain tissue, but also to enter neuronal cell cytoplasm and support microglia polarization into neuroprotective microglia, suggesting that RNPs protect the neurovascular unit and significantly improve the survival rate and neurological deficit. In the future, we plan to evaluate microglia polarization 7–14 days post-injection of medicines.

Using MULTIS method, we confirmed that intra-arterial injection of RNPs improved scavenging activities of OH, RO and ROO radicals. (Fig.12) We believe that RNPs suppress initial superoxide production; however, compared with edaravone, RNPs significantly suppress and inhibit further radical chain reactions that lead to OH, RO, and ROO production. This inhibition could be the main pillar of protective effect of RNPs and the key to their superiority compared with edaravone. By measuring the fluorescence of MitoSOX™ Red positive cells in the in the peri-infarction area, we confirmed that RNPs significantly improved scavenging activity of mitochondrial superoxide radical compared to edaravone. (Fig.13, 14) Mitochondria are power generators of every living cell and have a key role in the cell energy homeostasis. Different mechanisms of cell death, including apoptosis and autophagy, are mediated through the mitochondria. Following ischemia-reperfusion injury, generated superoxide anion in the mitochondria reacts with the nitrogen oxide and forms peroxynitrite anion, powerful radical that can causes the formation of other cytotoxic radicals and modifications in the cellular DNA,

proteins, and lipids. Ischemia-reperfusion injury is characterised by mitochondrial dysfunction that can induce neuronal cell death. [38-43] RNP by scavenging mitochondrial superoxide radical, protects mitochondria and its function, and this role of RNP could be crucial for survival of neurons in the peri-infarction area and neurological improvement recorded 24 h after the injection of RNPs.

5.4. Limitations and future challenges

This study had several limitations. First, we used a male mouse tMCAO model. This model can mimic but not replicate the pathophysiology of human large brain vessel occlusion. Liu et al. discuss the “female-protected” phenotype that has been described in preclinical studies. Furthermore, they identify “sexual dimorphism in stroke” that has been described in female rats and mice that developed smaller brain damage after “equivalent insult by focal or global cerebral ischemia compared to males”. [44,45] Therefore, to be able to study stroke in aged animals both sexes should be included. Additionally, as described by Liu et al. inducing MCAO is far more difficult in aging mice than in young ones. Aging mice are heavier with more visceral fat and are therefore less tolerant to anesthesia. Additionally, blood vessels of older mice are less flexible and insertion of the occluding filament is difficult. This leads to higher mortality following MCAO. tMCAO in aging mice is not a simple surgical procedure, and when combined with high cost of purchasing and raising animals, it is not hard to understand why many researchers avoid conducting studies in middle-aged and aging animals. [44,45] Second, we injected RNPs 20 min after reperfusion, narrowing the therapeutic time window. Owing to the possibility that cerebral infarction might expand 24 h after the injection of RNPs, future studies should include the evaluation of survival rate, neurological deficits, infarct area size for up to 7 days after the injection

of RNPs and edaravone. Third, we detected RNPs 24 h post-injection, but we did not know the changes in RNPs distribution that occur with time or their in vivo pharmacodynamics. All of these limitations should be resolved in future in order to develop RNPs for the clinical use.

For RNPs to enter into clinical stage of examination it is necessary to evaluate the mechanism of RNPs internalization into the cytoplasm of the neuron cells, elucidate RNPs effect on the oxidative stress disorder in neurons and neuronal mitochondria and evaluate the neuroprotective effect of RNPs using a large animal stroke model, such as Cynomolgus monkey tMCAO model.

CHAPTER 6 CONCLUSION

RNPs are a useful type of nanoparticles for the treatment of cerebral ischemia-reperfusion injury. With a significantly better survival rate, neurological deficit, BBB protection, and ROS-scavenging capacity, RNPs are undoubtedly superior compared with the already marketed free-radical scavenger edaravone.

RNPs, with their cytoplasmic distribution, could be the future antioxidant and neuroprotective nanomedicine and treatment for cerebral ischemia-reperfusion injury after mechanical thrombectomy in acute ischemic stroke. (Fig.15)

CHAPTER 7 FIGURE LEGENDS

Fig.1. Schematic representation of redox-nanoparticles RNPs design (A) and pH responsiveness of RNPs (B).

Fig.2. Dose-dependent RNP and edaravone efficiency pilot studies. (A, B) Survival rate and neurological deficit Longa score 24 h post-injection of 0.09 mg/kg, 0.9 mg/kg, and 9 mg/kg of RNP ($n = 6$ each), control group was given phosphate-buffered saline (PBS; $n = 6$) $*P < 0.05$. (C, D) Survival rate and neurological deficit Longa score 24 h post-injection of 0.03 mg/kg, 0.3 mg/kg, and 3 mg/kg of edaravone ($n = 6$ each), control group was given phosphate-buffered saline (PBS; $n = 6$) $*P < 0.05$; n.s., no significant difference. RNP, nitroxide radical-containing nanoparticle. PBS, phosphate-buffered saline.

Fig.3. Schematic representation of experiment timeline and tMCAO in mice.

Fig.4. RNPs significantly improved the survival rate and neurological deficit 24 h post-injection. (A) Survival rate 24 h post-injection of PBS ($n = 12$), edaravone ($n = 20$) and RNP ($n = 20$); $*P < 0.05$. (B) Neurological deficit Longa score 24 h post-injection of PBS ($n = 12$), edaravone ($n = 20$) and RNP ($n = 20$); $*P < 0.05$. (C) Neurological deficit NSS-R score 24 h post-injection of PBS ($n = 4$), edaravone ($n = 4$) and RNP ($n = 4$); $*P < 0.05$. (D) Rotarod test, seconds taken for animals to fall of the rotarod device 24 h post-injection of PBS ($n = 4$), edaravone ($n = 4$) and RNP ($n = 4$); $*P < 0.05$. RNP, nitroxide radical-containing nanoparticle. PBS, phosphate-buffered saline.

Fig.5. RNPs significantly inhibited BBB disruption. (A) Representative pictures of EB extravasation in an ischemic brain area 24 h post-injection of medicines. (B) Quantitative analysis of EB leakage. EB concentration is presented as $\mu\text{g/g}$ ischemic brain hemisphere: edaravone group ($n = 4$) and RNP group ($n = 4$); $*P < 0.05$. (C) Brain permeability index expressed as 10^{-3} mL/g of

ischemic brain hemisphere 24 h post-injection of PBS ($n = 4$), edaravone ($n = 4$) and RNP ($n = 4$); $*P < 0.05$. RNP, nitroxide radical-containing nanoparticle; BBB, blood-brain barrier; EB, Evans blue.

Fig.6. Anti-rhodamine-labeled RNPs were detected in endothelial cells, the perivascular space, neuronal cell cytoplasm, astrocytes, and microglia. Representative fluorescent images of the peri-infarction area (magnification $\times 400$). **(A)** RNPs were localized in endothelial cells: green, CD31; red, Anti-rhodamine; and blue, DAPI. **(B)** RNPs were localized in the neuronal cell cytoplasm: red, NeuN; green, Anti-rhodamine; and blue, DAPI. **(C)** RNPs were localized around astrocytes surrounding brain blood vessels: green, GFAP; red, Anti-rhodamine; and blue, DAPI. **(D)** RNPs were localized around microglia: red, iba-1; green, Anti-rhodamine; and blue, DAPI. RNPs, nitroxide radical-containing nanoparticles; DAPI, 4',6-diamidino-2-phenylindole; GFAP, glial fibrillary acidic protein. Bar, 50 μm .

Fig.7. Rhodamine-labeled RNPs were distributed around NeuN-positive cells and in NeuN-positive cell cytoplasm and in brain blood vessels surrounded by astrocytes **(A)**. Representative fluorescent images **(A)** and confocal microscope image **(B)** of the peri-infarction area (magnification $\times 400$). Red, NeuN; green, Anti-rhodamine; and blue, DAPI. **(B)** Arrow: RNPs in brain blood vessels; arrowhead: RNPs in NeuN cell cytoplasm. RNPs, nitroxide radical-containing nanoparticles. Rhodamine-labeled RNPs were found in brain blood vessels and in the perivascular space (arrow) and in NeuN-positive cell cytoplasm (arrowhead). Representative 3D and z -stack analysis **(C)** fluorescent images of the peri-infarction area (magnification $\times 1000$). Red, NeuN; green, Anti-rhodamine; and blue, DAPI. RNPs, nitroxide radical-containing nanoparticles; DAPI, 4',6-diamidino-2-phenylindole.

Fig.8. Representative fluorescent images of the peri-infarction area of control group (PBS-treated mice) (magnification 400×). **(A)** Anti-rhodamin was not found in endothelial cells: green, CD31; red, Anti-rhodamine; and blue, DAPI. **(B)** Anti-rhodamin was not localized in the neuronal cell cytoplasm: red, NeuN; green, Anti-rhodamine; and blue, DAPI. **(C)** Anti-rhodamin was not found around astrocytes: green, GFAP; red, Anti-rhodamine; and blue, DAPI. **(D)** Anti-rhodamine was not found around microglia: red, iba-1; green, Anti-rhodamine; and blue, DAPI. PBS, phosphate-buffered saline. DAPI, 4',6-diamidino-2-phenylindole; GFAP, glial fibrillary acidic protein.

Fig.9. Perivascular EB extravasation. Representative images of the peri-infarction area (magnification ×400). RNP group ($n = 4$) **(A)** and edaravone group ($n = 4$) **(B)**. **(A)** EB extravasation around brain blood vessels: green, CD31; red, EB; blue, Anti-rhodamine; and light blue, DAPI. **(B)** EB extravasation around brain blood vessels: green, CD31; red, EB; blue, DAPI. EB, Evans blue; RNP, nitroxide radical-containing nanoparticle; DAPI, 4',6-diamidino-2-phenylindole. Bar, 50 μm.

Fig.10. RNPs supported microglia polarization into microglia M2. **(A)** Total number of microglia M2 cells in the peri-infarction area (cells/mm²): RNP group ($n = 4$) and edaravone group ($n = 4$); * $P < 0.05$. Representative images of the peri-infarction area (magnification ×400). **(B)** RNP group: yellow fluorescence indicates double-positive microglia M2 cells; green, CD206; red, iba-1; and blue, Anti-rhodamine. Edaravone group: significantly fewer double-positive microglia M2 cells; green, CD206; red, iba-1; and blue, DAPI. **(C)** Total number of microglia M1 cells in the peri-infarction area (cells/mm²): RNP group ($n = 4$) and edaravone group ($n = 4$). n.s., no significant difference; $P = 0.21$. **(D)** RNP group: yellow fluorescence indicates double-positive microglia M1 cells; green, CD16/32; red, iba-1; and blue, DAPI. Edaravone group: microglia M1 cells; green,

CD16/32; red, iba-1; and blue, DAPI. RNP, nitroxide radical-containing nanoparticle; DAPI, 4',6-diamidino-2-phenylindole. Bar, 50 μ m.

Fig.11. Representative fluorescent images of the peri-infarction area of control group (PBS-treated mice) (magnification 400 \times). **(A)** Yellow fluorescence indicates double-positive microglia M1 cells; green, CD16/32; red, iba-1; and blue, DAPI. **(B)** Microglia M2 cells; green, CD206; red, iba-1; and blue, DAPI. PBS, phosphate-buffered saline. DAPI, 4',6-diamidino-2-phenylindole.

Fig.12. RNPs improved multiple ROS-scavenging capacity in the ischemic brain. ROS-scavenging capacity in the ischemic brain 24 h post-injection of RNP ($n = 4$) and edaravone ($n = 4$). **(A)** Hydroxyl radical-scavenging capacity presented as mM-GSHeq; $*P < 0.05$. **(B)** Alkoxy radical-scavenging capacity presented as mM-Troloxeq; $*P < 0.05$. **(C)** Alkyl peroxy radical-scavenging activity presented as μ M- α -LAEq; $*P < 0.05$. **(D)** Superoxide radical-scavenging activity presented as U/mL-SODEq. n.s., no significant difference; $P = 0.27$. RNP, nitroxide radical-containing nanoparticle; ROS, reactive oxygen species; GSH, glutathione; SOD, superoxide dismutase.

Fig.13. RNPs improved mitochondrial superoxide scavenging capacity in the ischemic brain. **(A)** Average corrected total cell fluorescence in the core of the infarction area 24 h post-injection of RNP ($n = 4$), edaravone ($n = 4$) and PBS ($n = 4$); n.s., no significant difference; $P = 0.15$. **(B)** Average corrected total cell fluorescence in the peri-infarction area 24 h post-injection of RNP ($n = 4$), edaravone ($n = 4$) and PBS ($n = 4$); $*P < 0.05$. RNP, nitroxide radical-containing nanoparticle. PBS, phosphate-buffered saline.

Fig.14. Representative images of the peri-infarction area and the core of the infarction area (magnification $\times 1000$). RNP group ($n = 4$) **(A)**; edaravone group ($n = 4$) **(B)** and control group

(PBS-treated mice) ($n = 4$) (C). Red, MitoSOX™ Red; green, MitoTracker® Green FM; and blue, DAPI. RNP, nitroxide radical-containing nanoparticle. PBS, phosphate-buffered saline; DAPI, 4',6-diamidino-2-phenylindole.

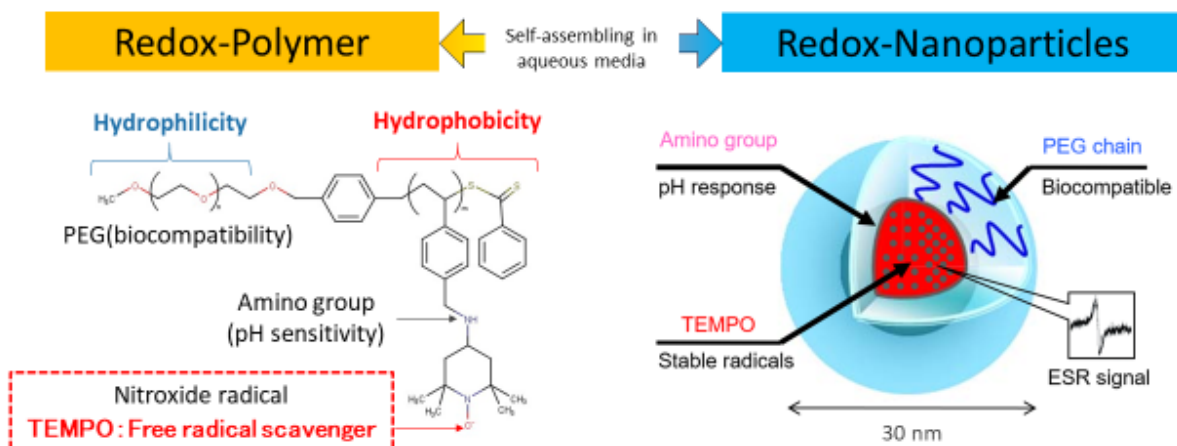
Fig.15. Schematic representation of redox-nanoparticles RNPs distribution and neuroprotective effects. After crossing the damaged BBB, RNPs are found in the perivascular space, supporting the integrity of the blood vessels and distributed around microglia and astrocytes. RNPs are also found internalized in the cytoplasm of the neuronal cells.

CHAPTER 8 FIGURES

Figure 1

(A)

REDOX NANOPARTICLES



T. Yoshitomi, Y. Nagasaki . Bioconjugate Chemistry. 2009

(B)

pH responsiveness

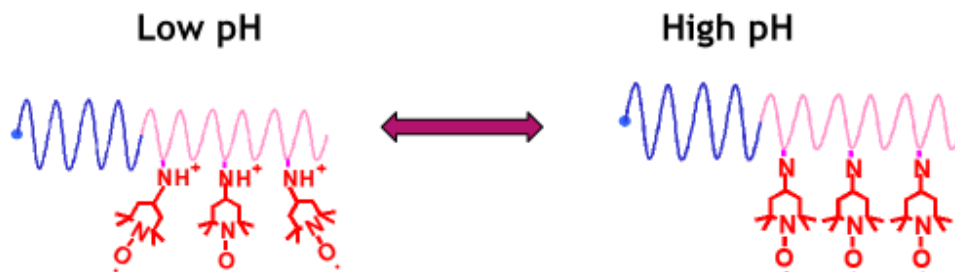
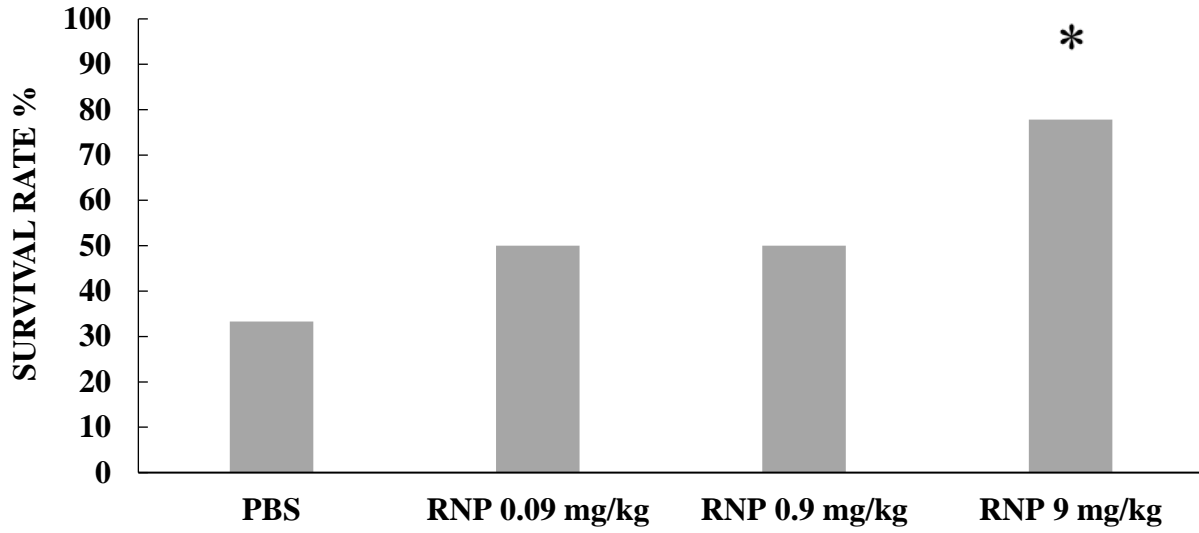
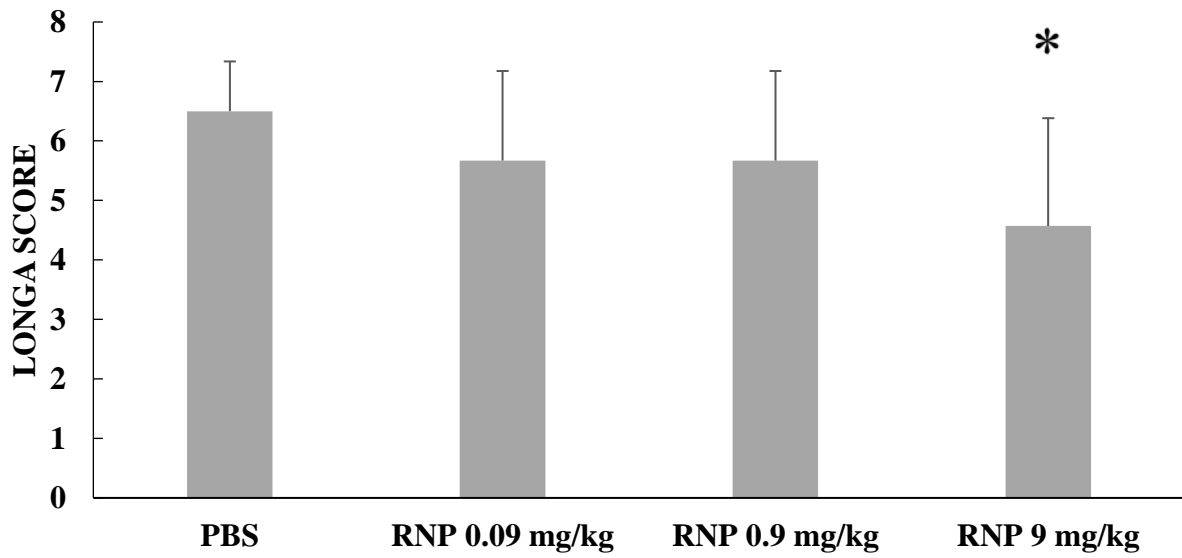


Figure 2

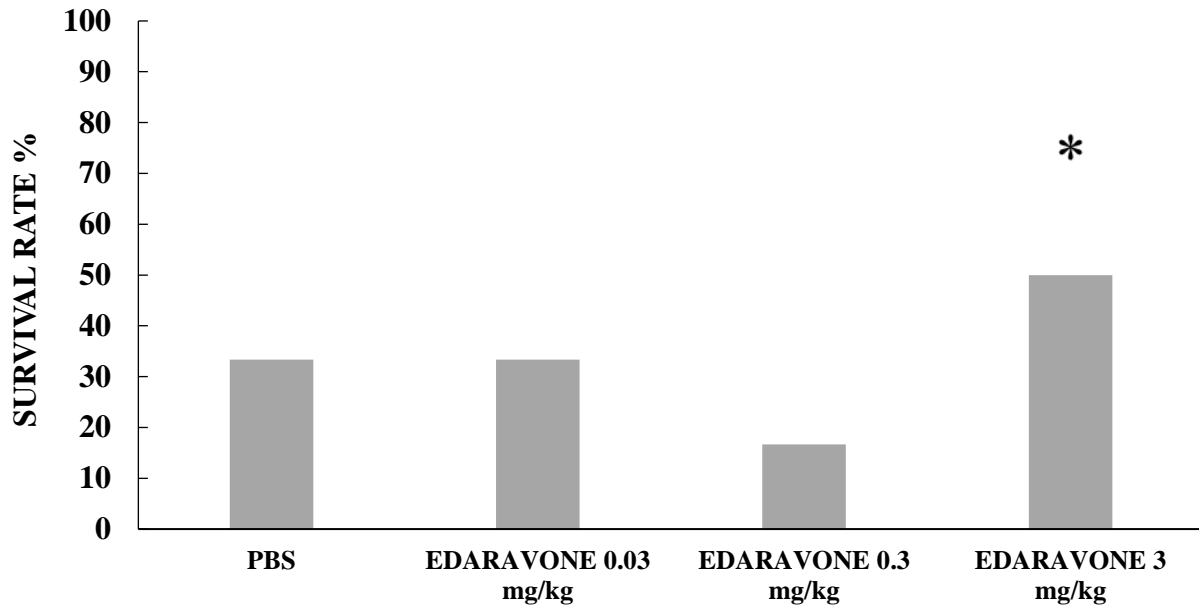
A



B



C



D

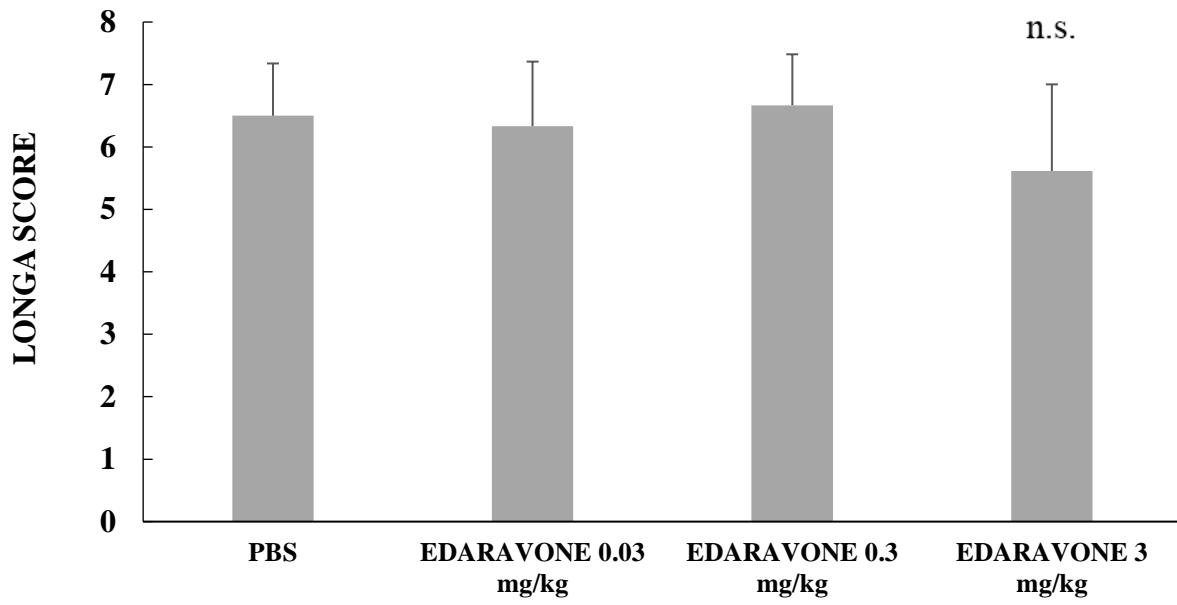


Figure 3

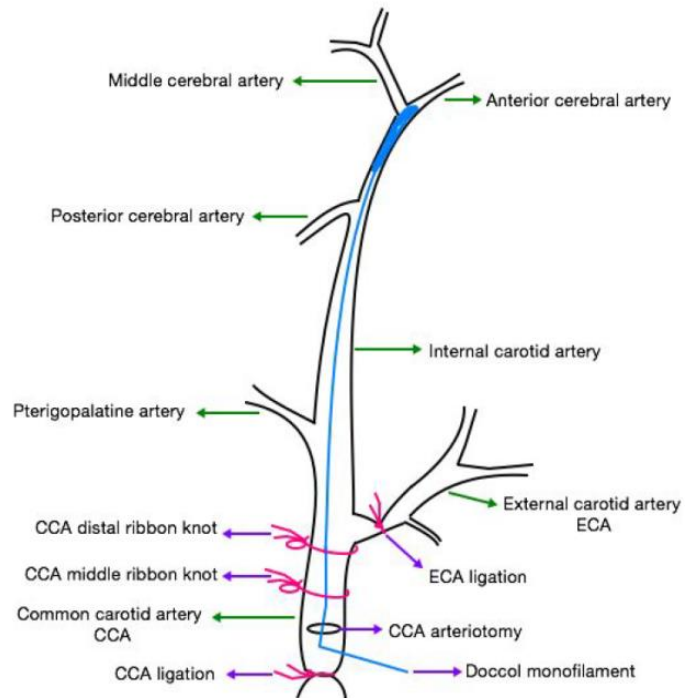
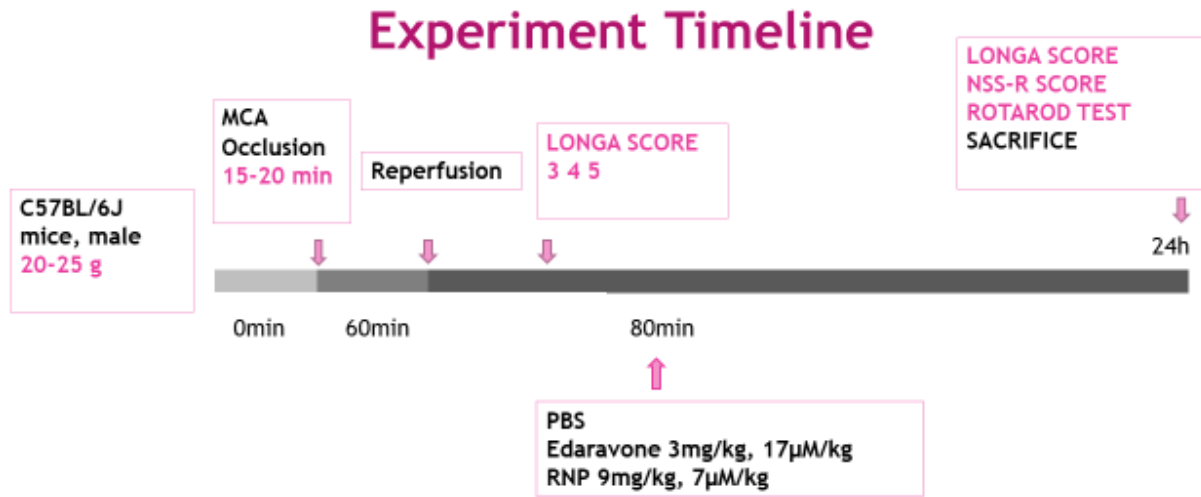
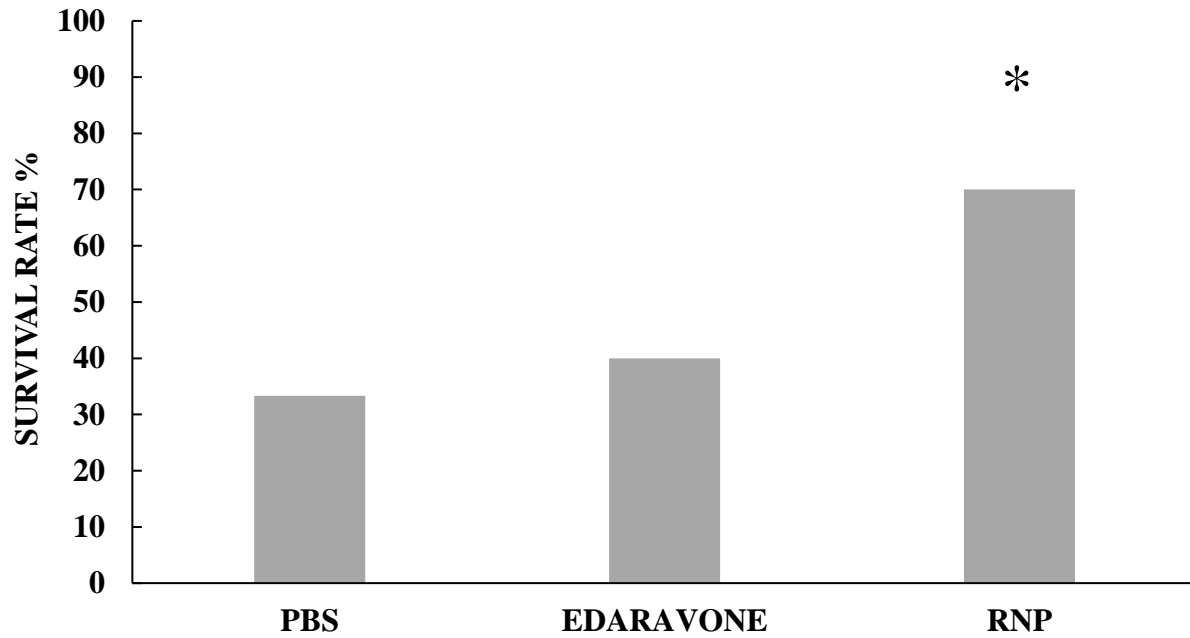
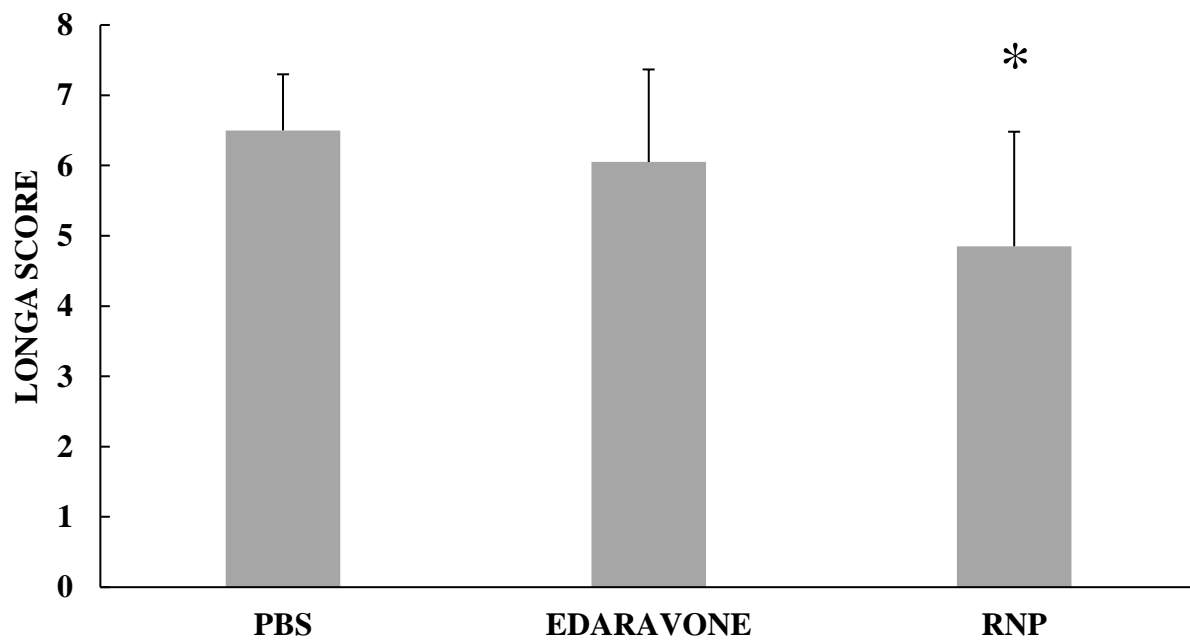


Figure 4

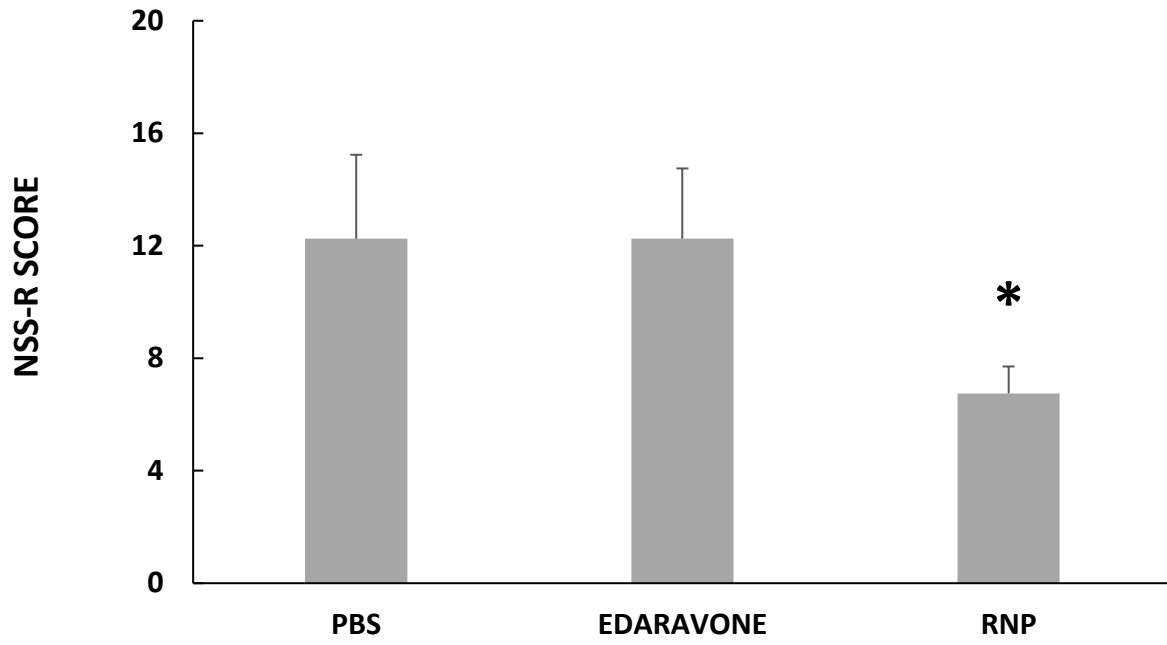
A



B



C



D

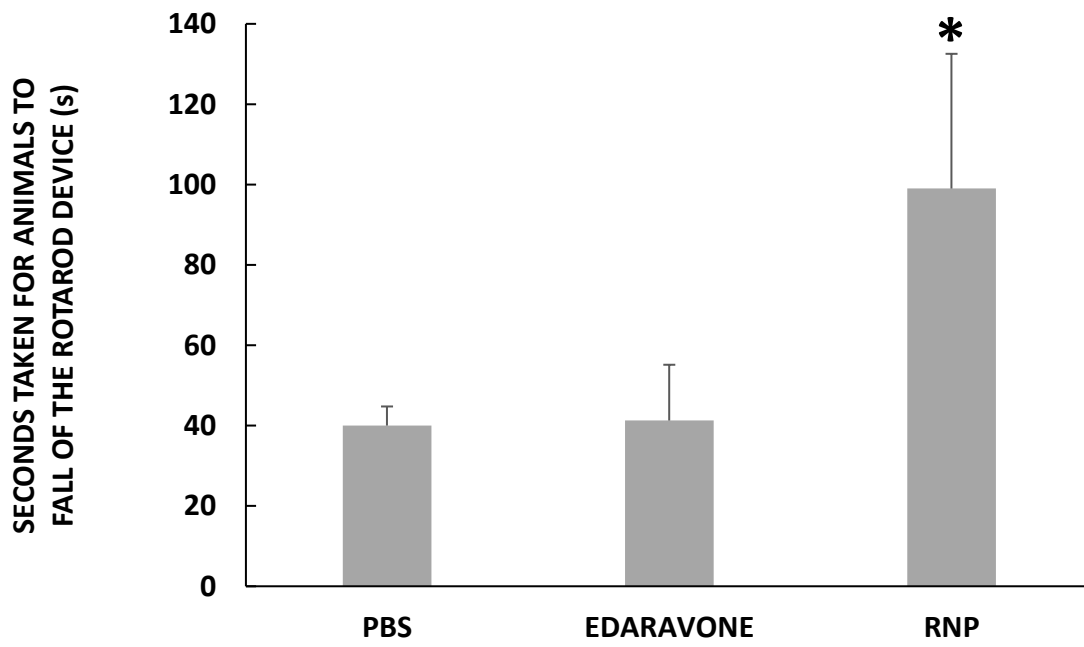
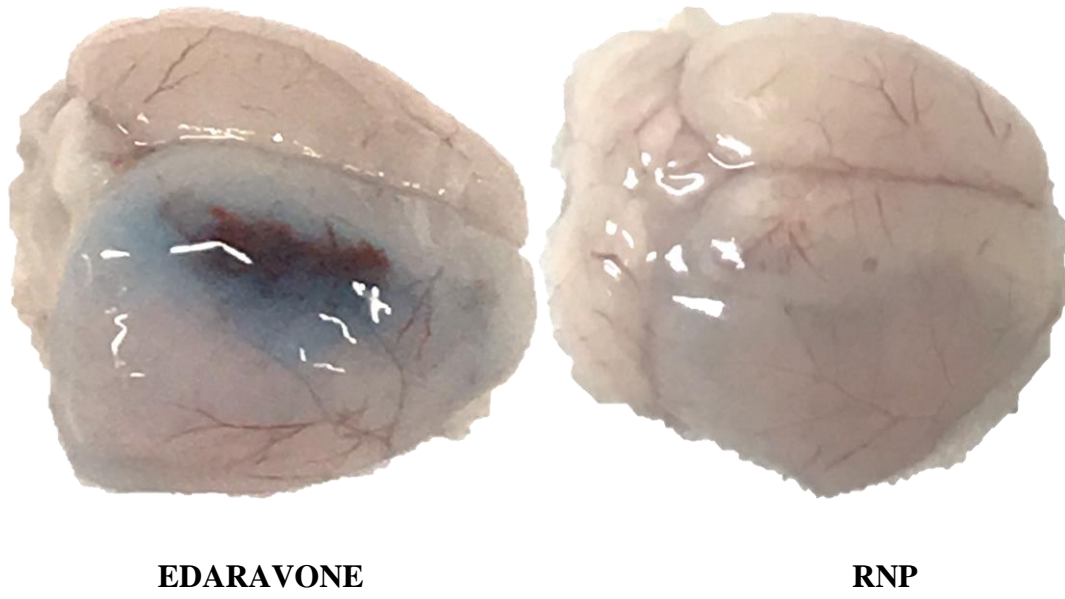
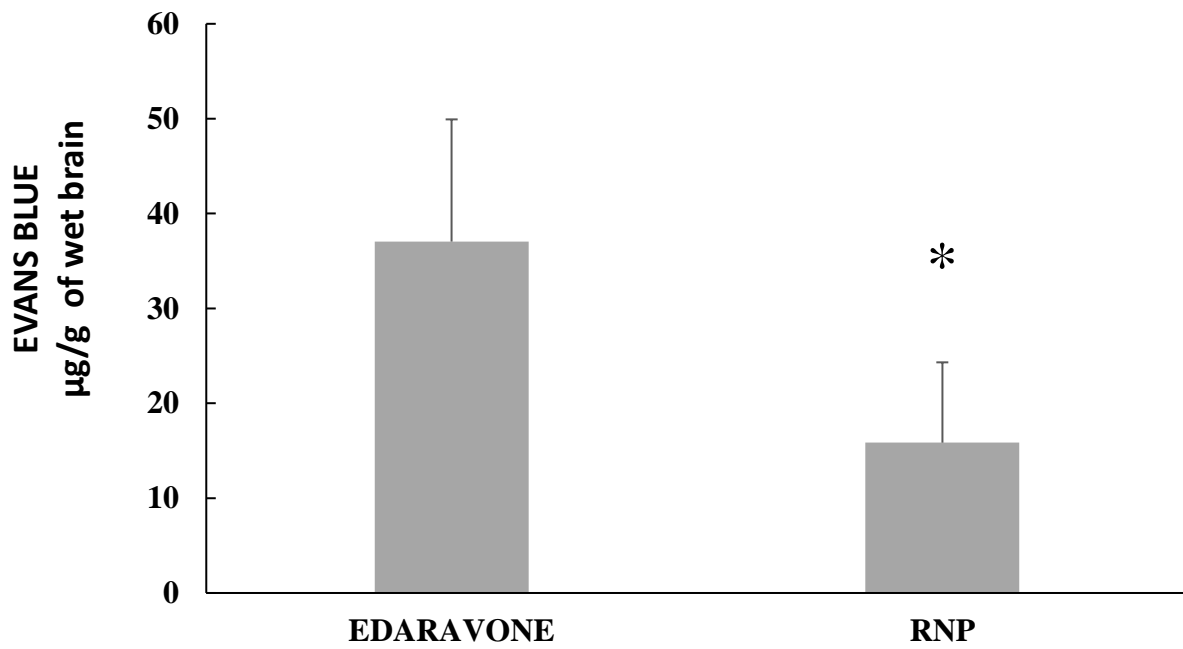


Figure 5

A



B



C

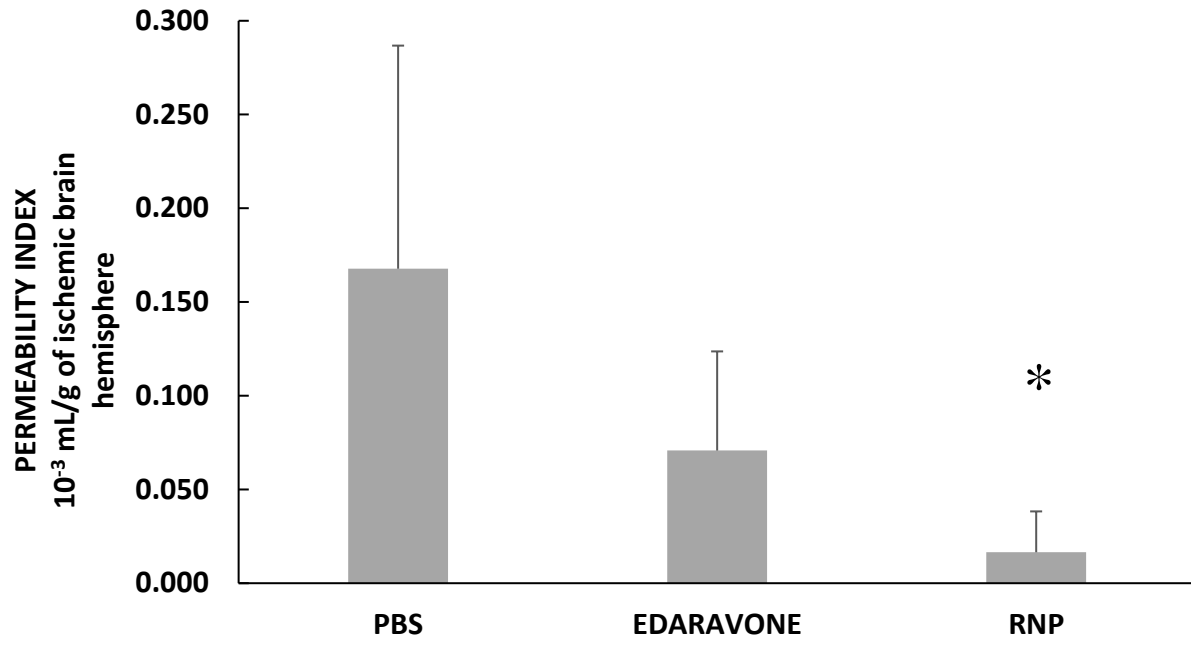
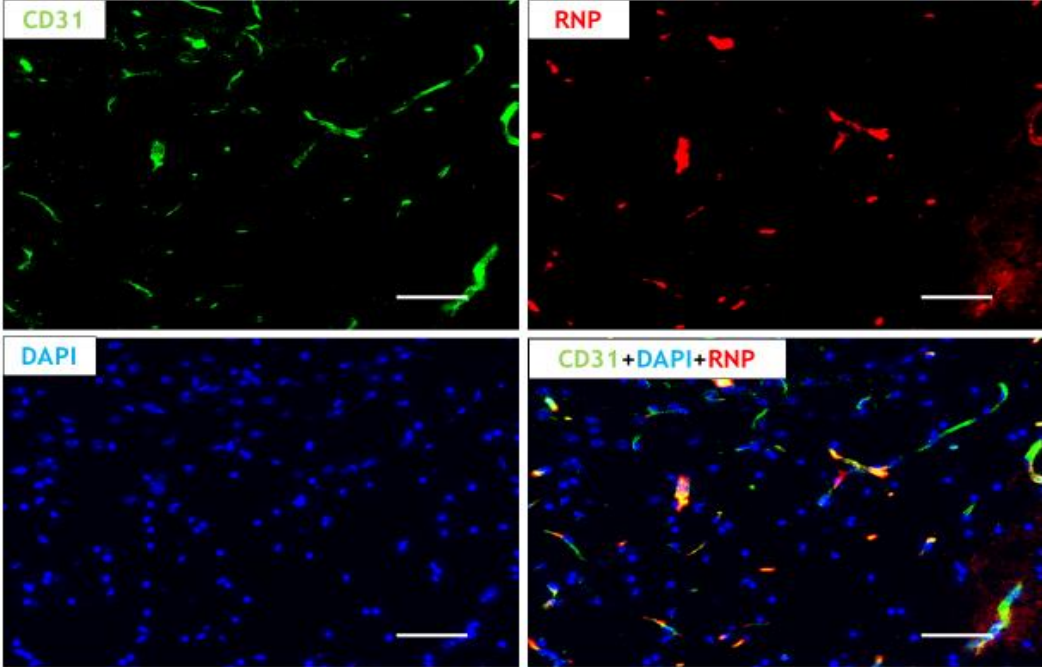
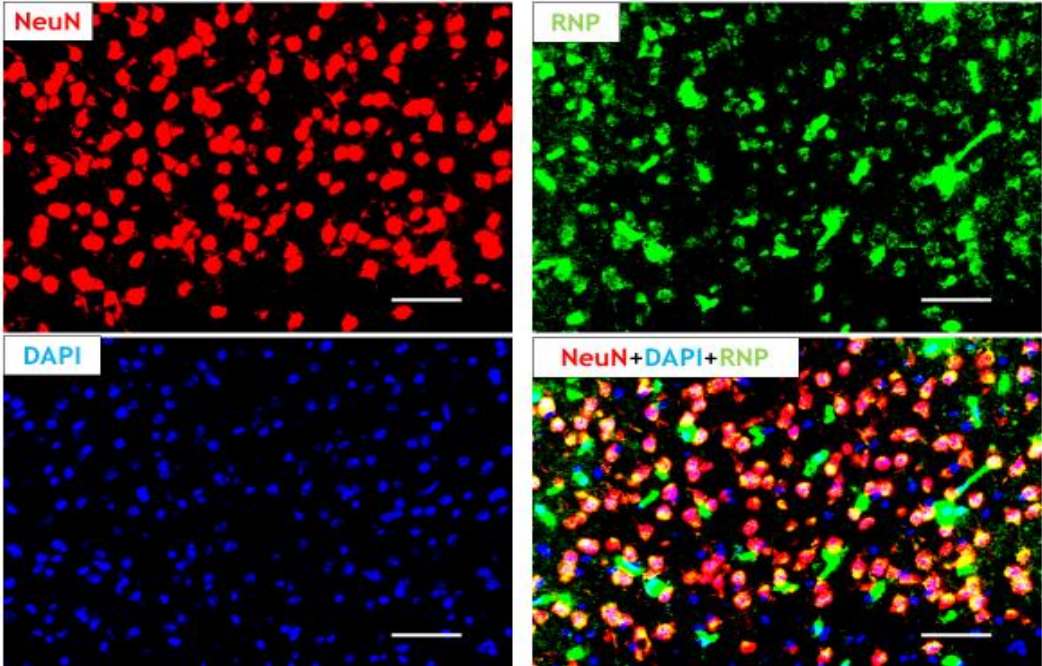


Figure 6

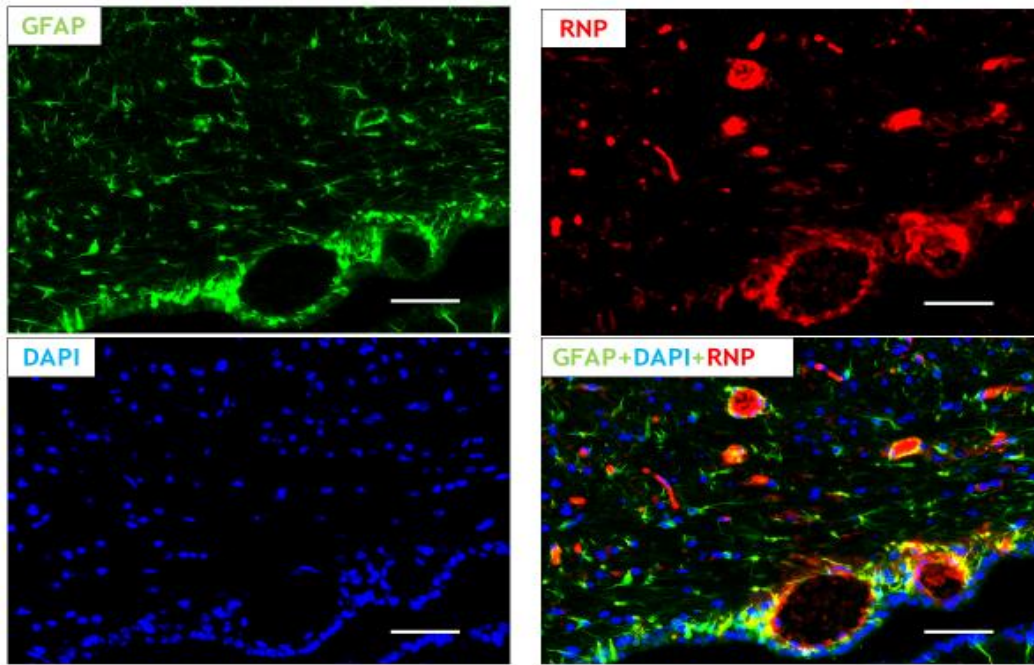
A



B



C



D

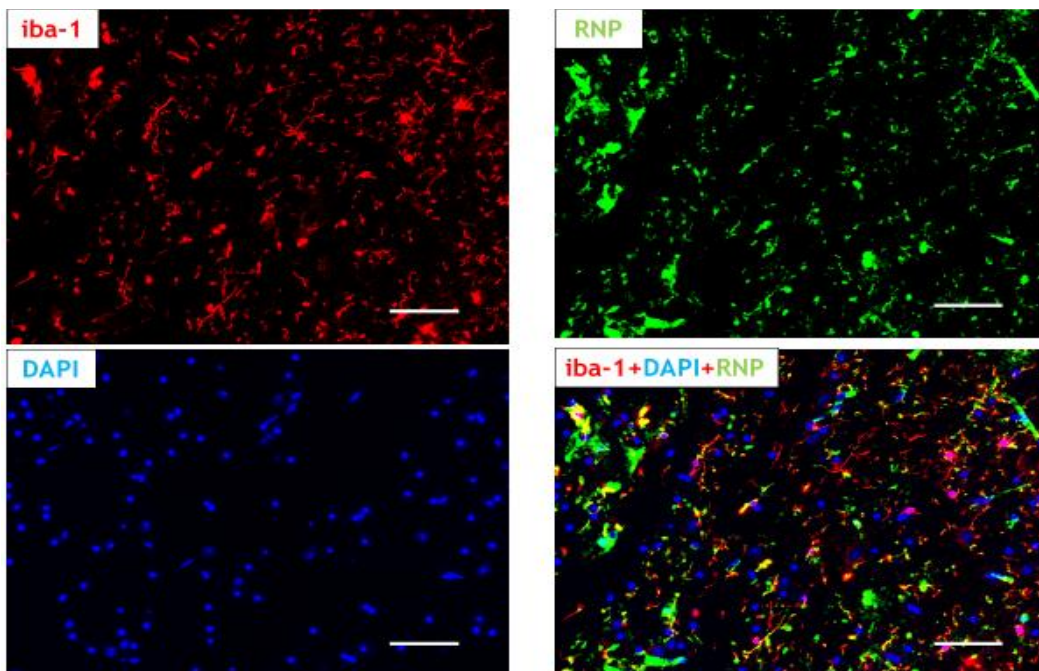
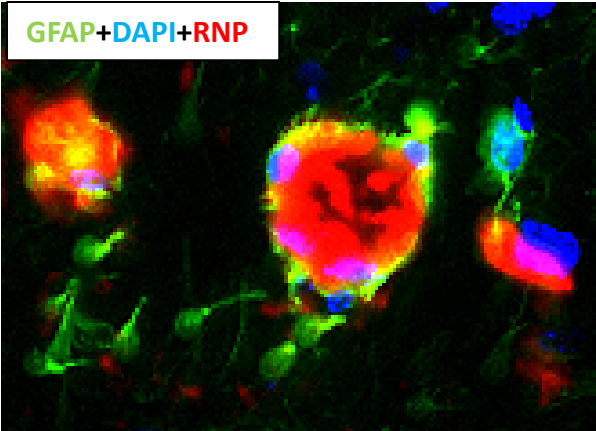
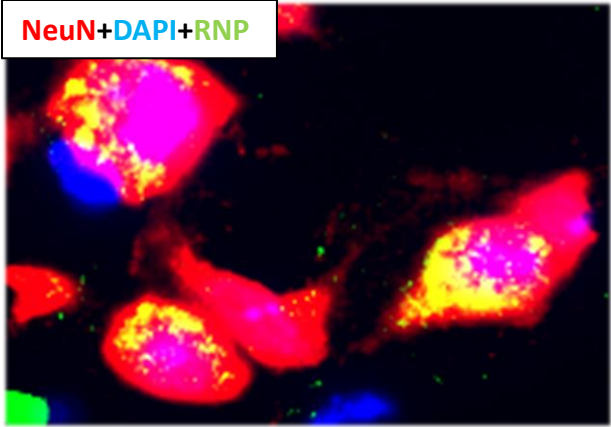
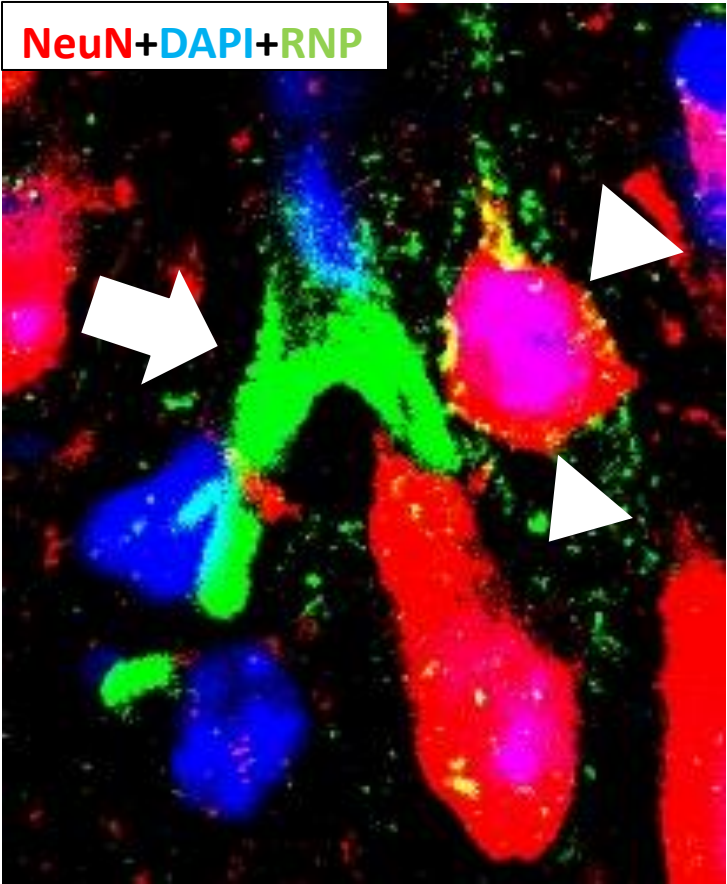


Figure 7

A



B



C

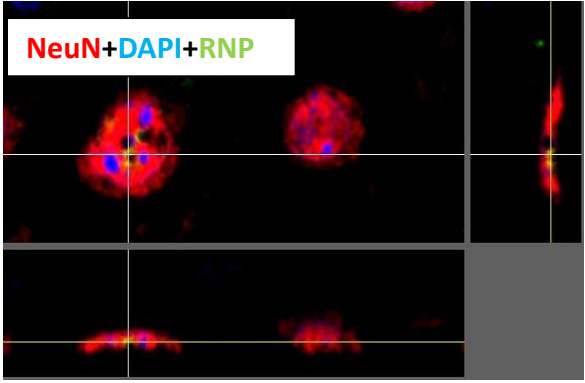
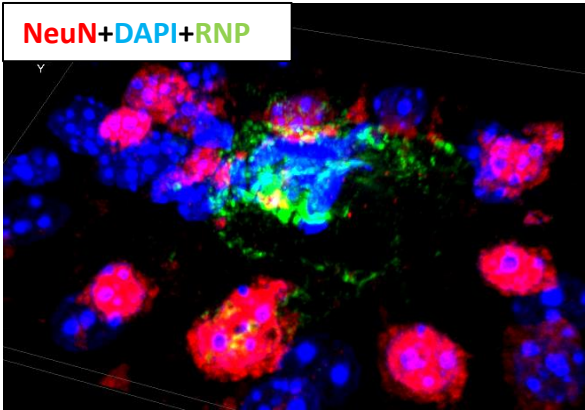
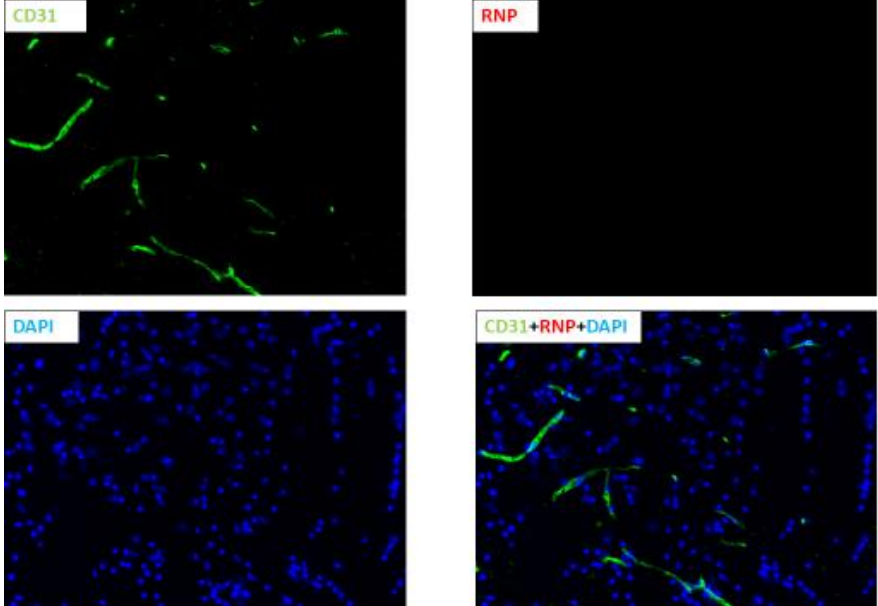
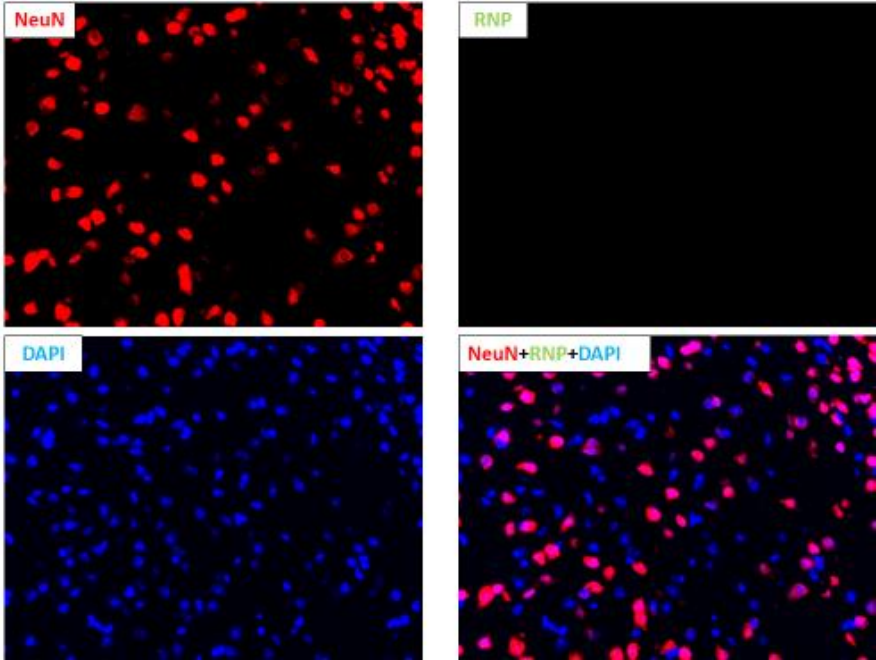


Figure 8

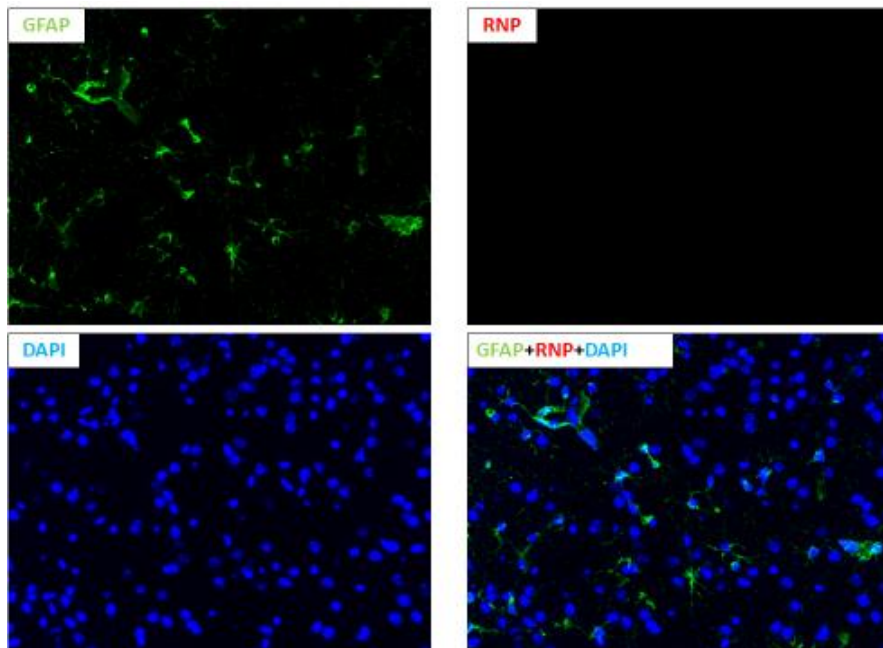
A



B



C



D

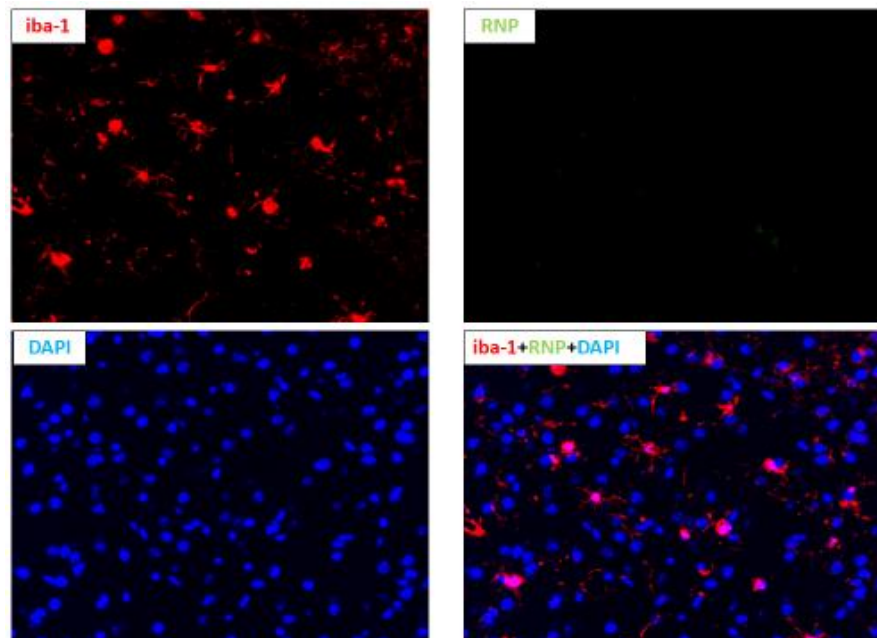
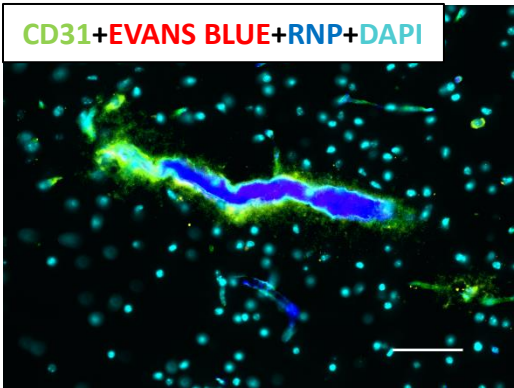
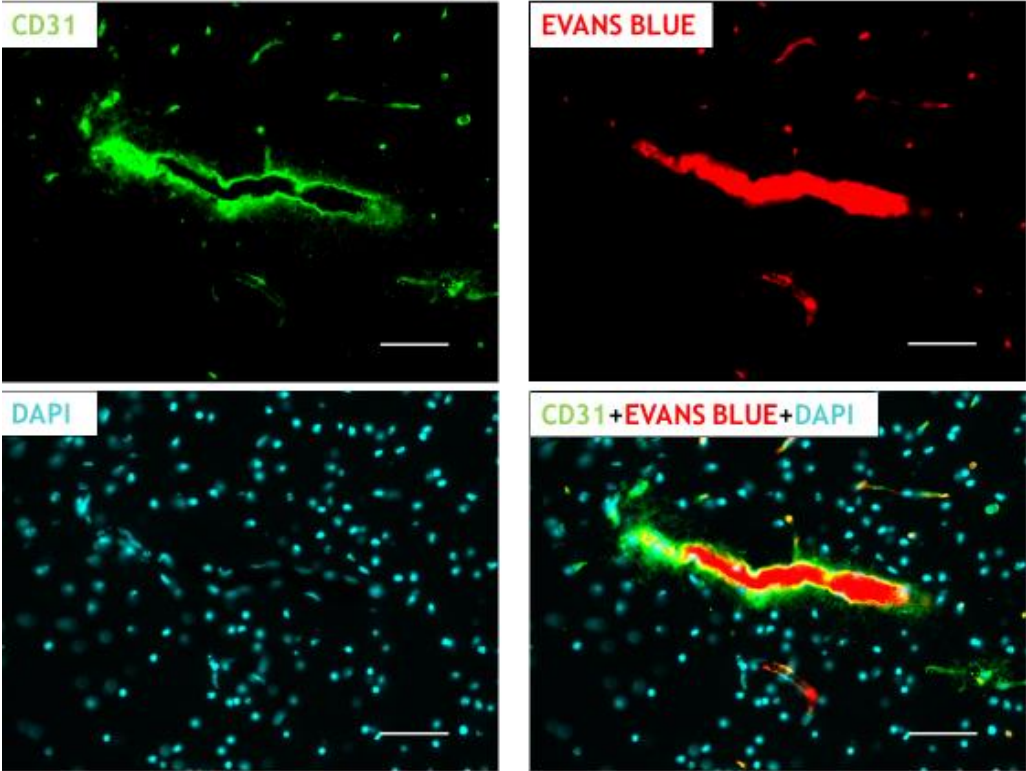


Figure 9

A



B

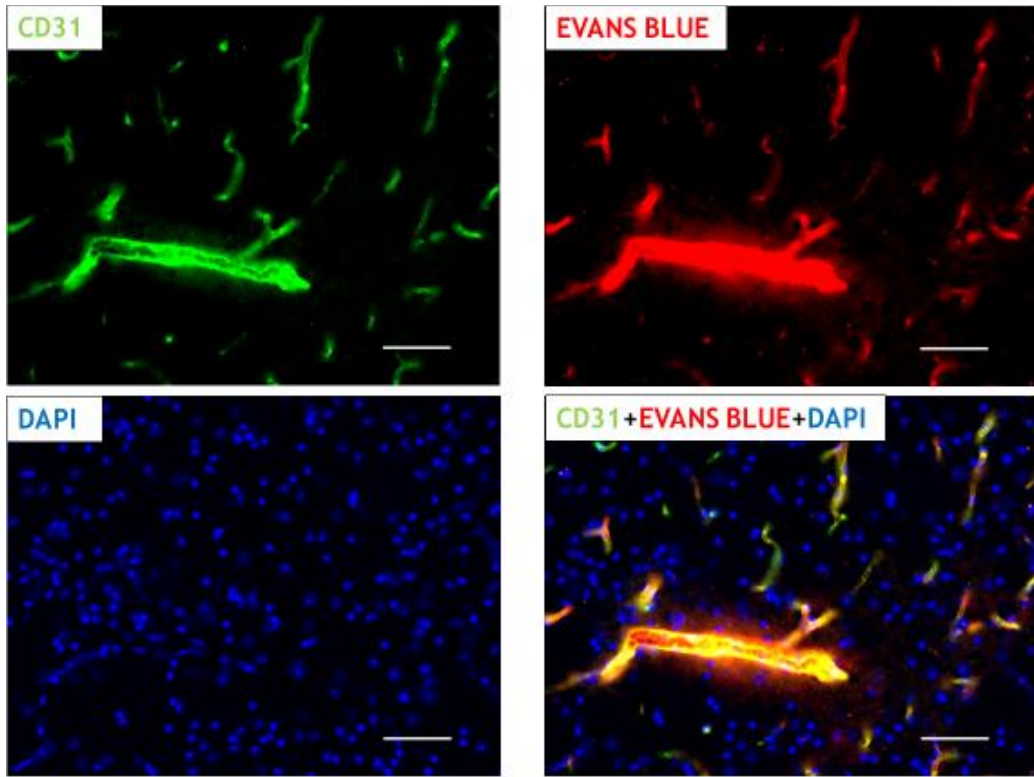
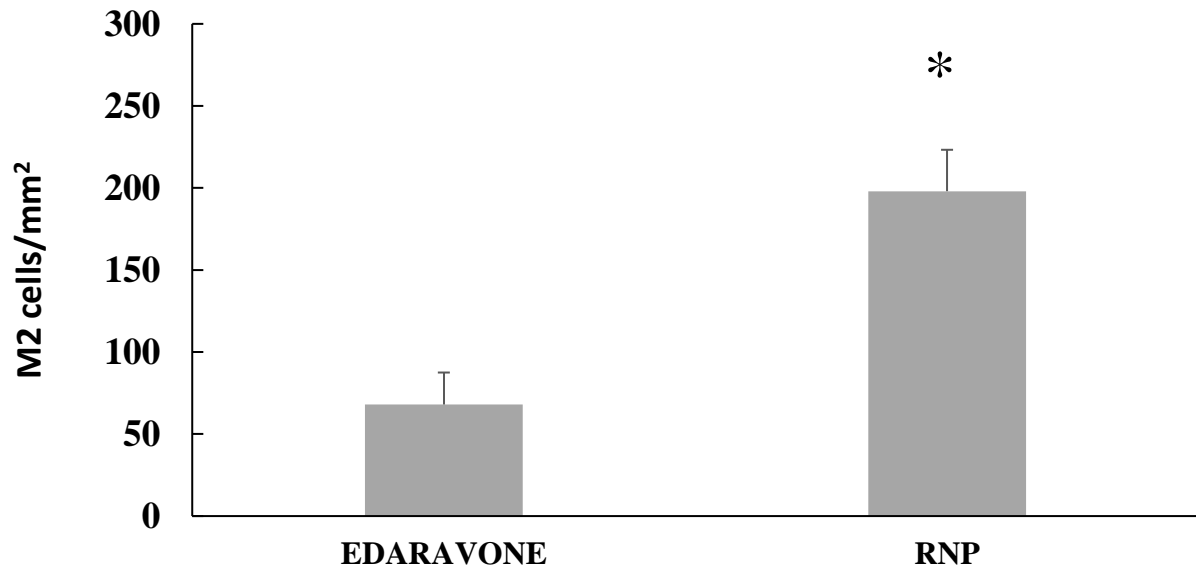
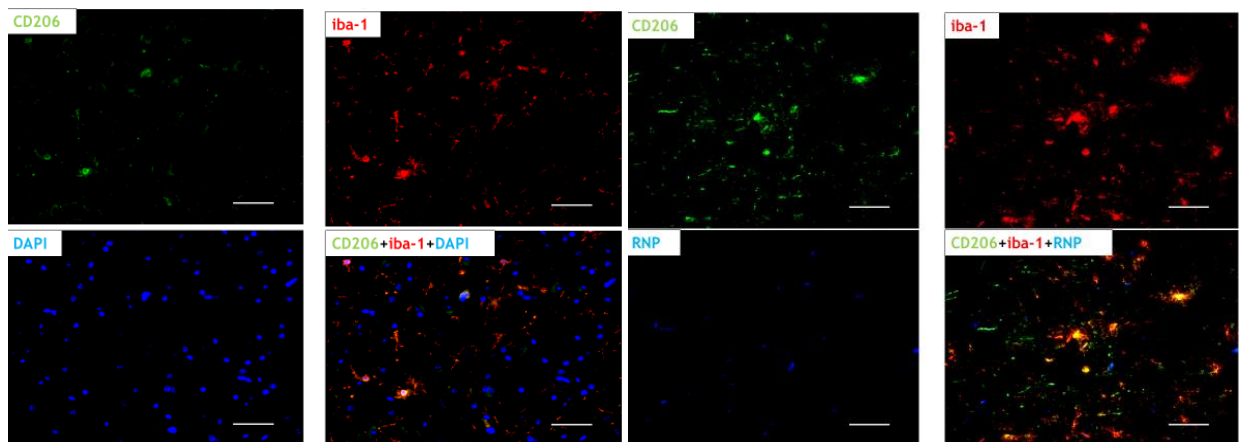


Figure 10

A



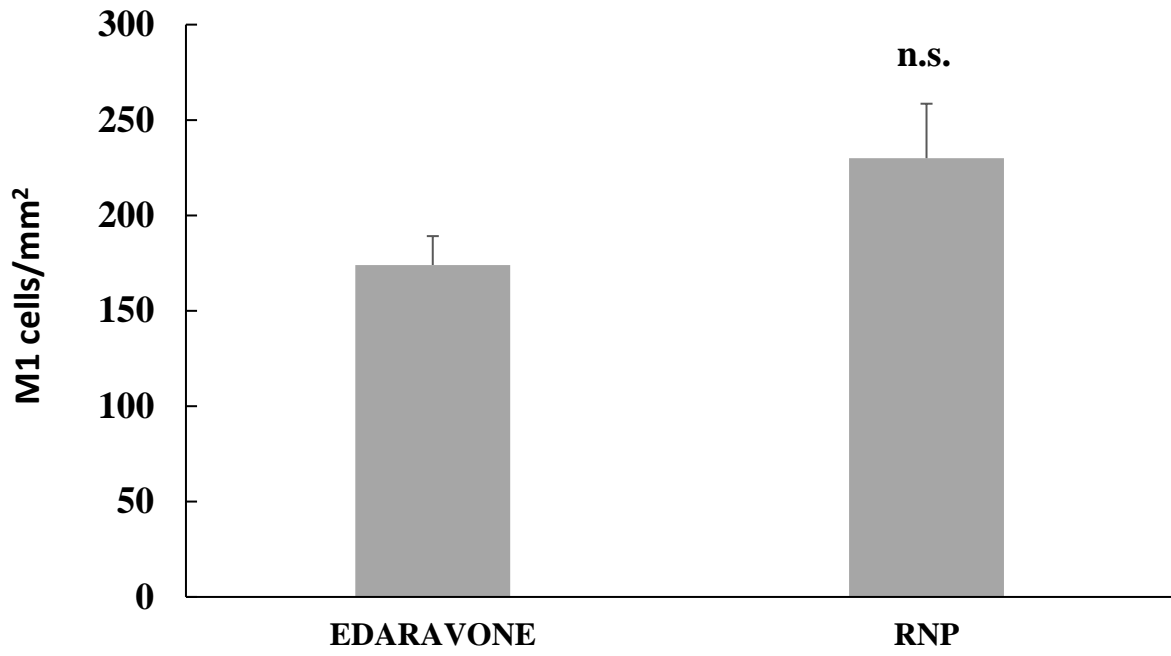
B



EDARAVONE

RNP

C



D

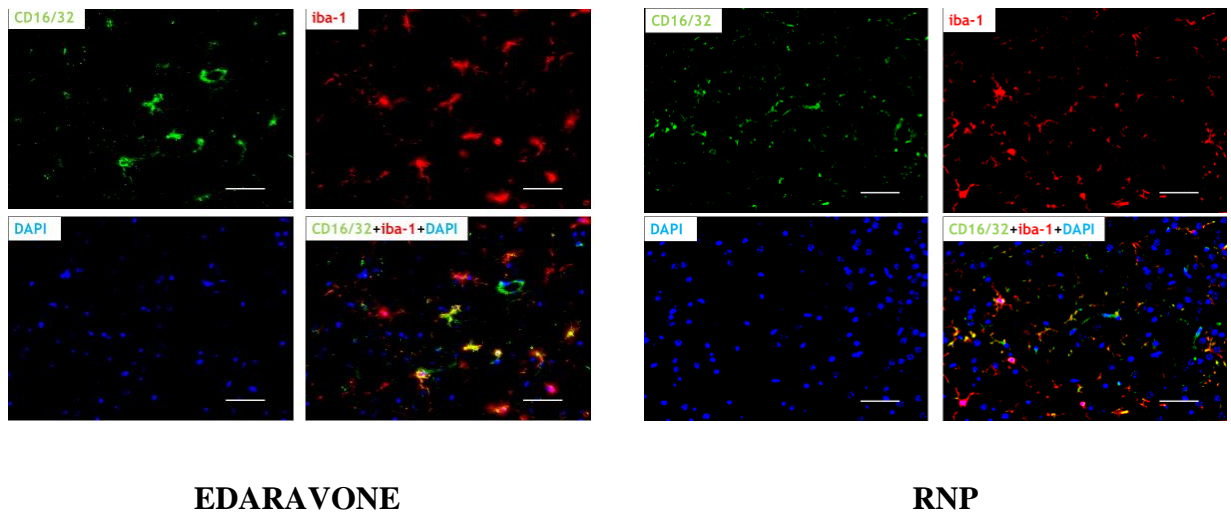
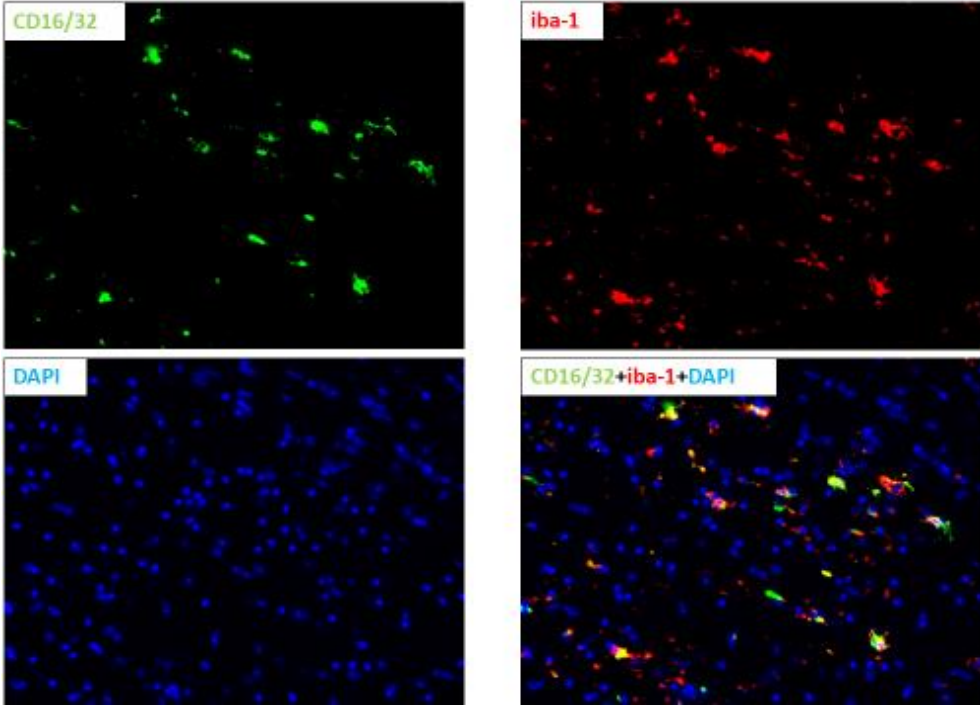


Figure 11

A



B

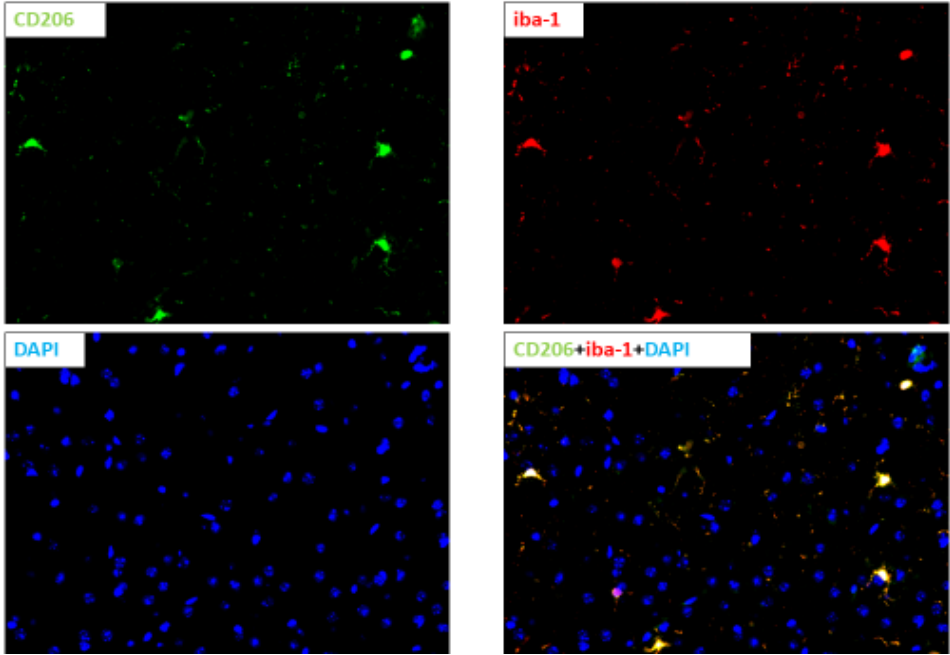
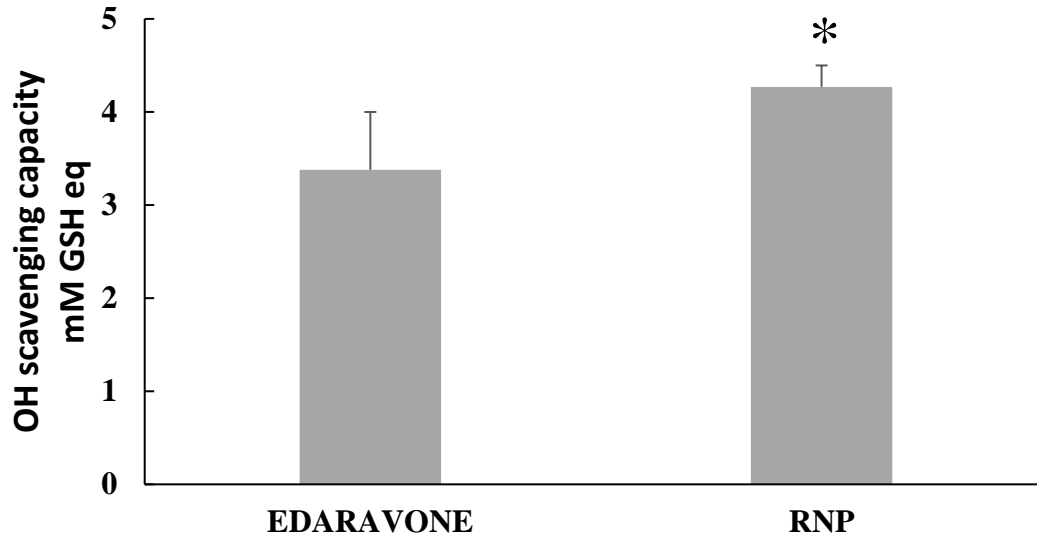
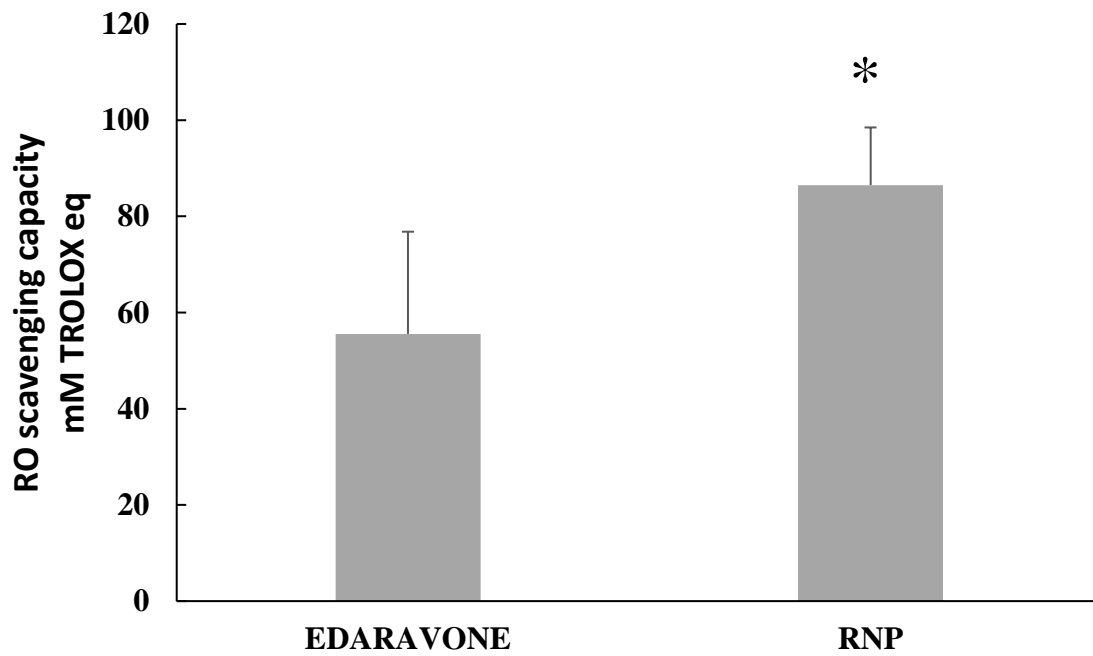


Figure 12

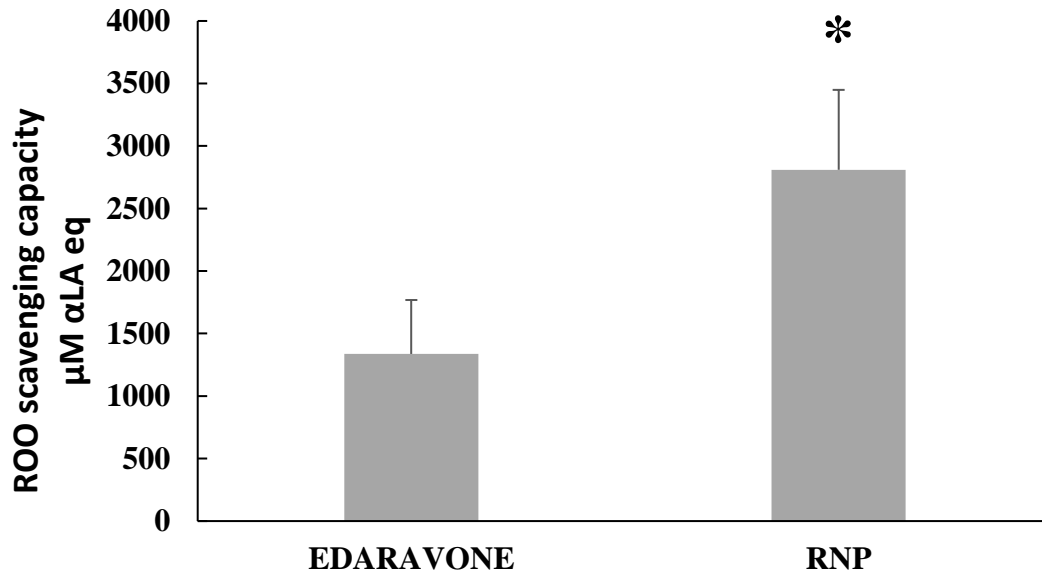
A



B



C



D

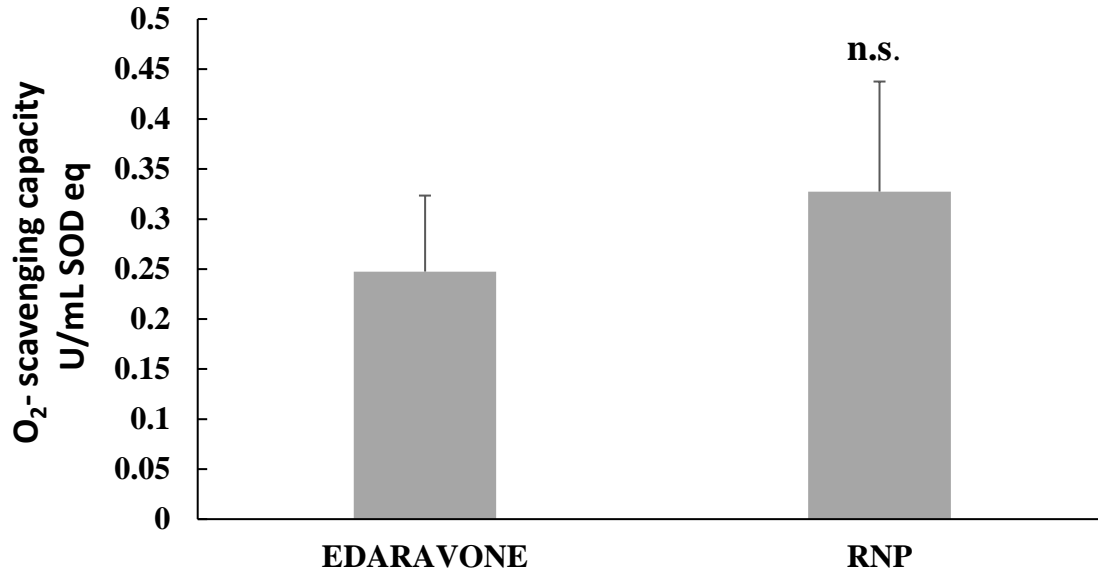
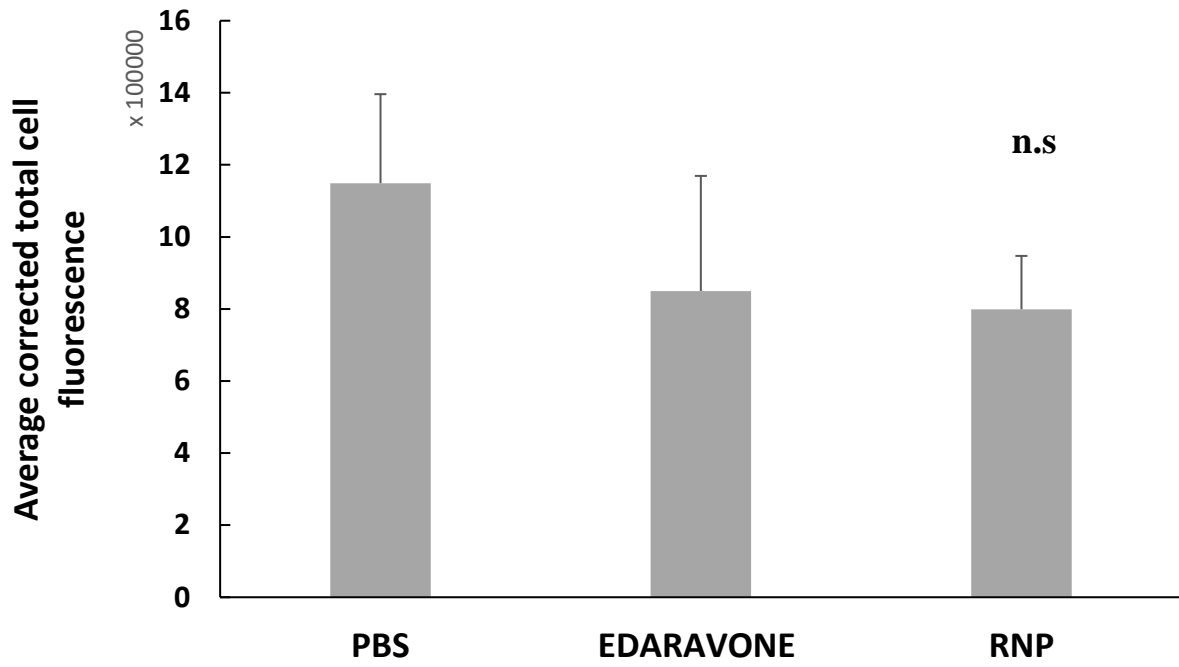


Figure 13

A



B

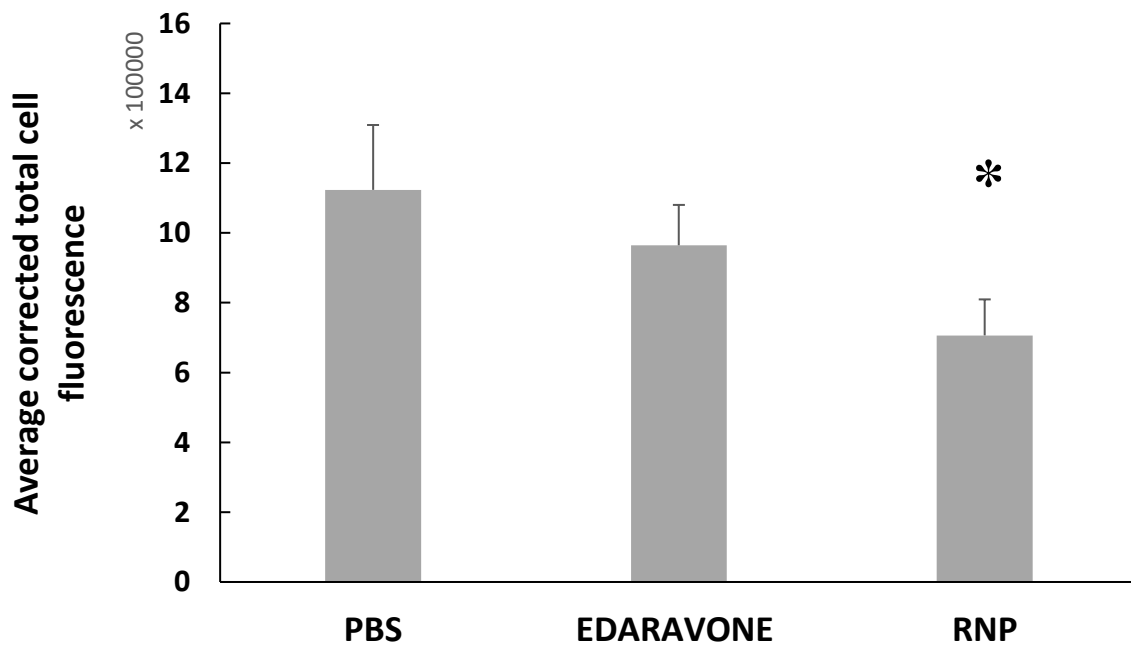
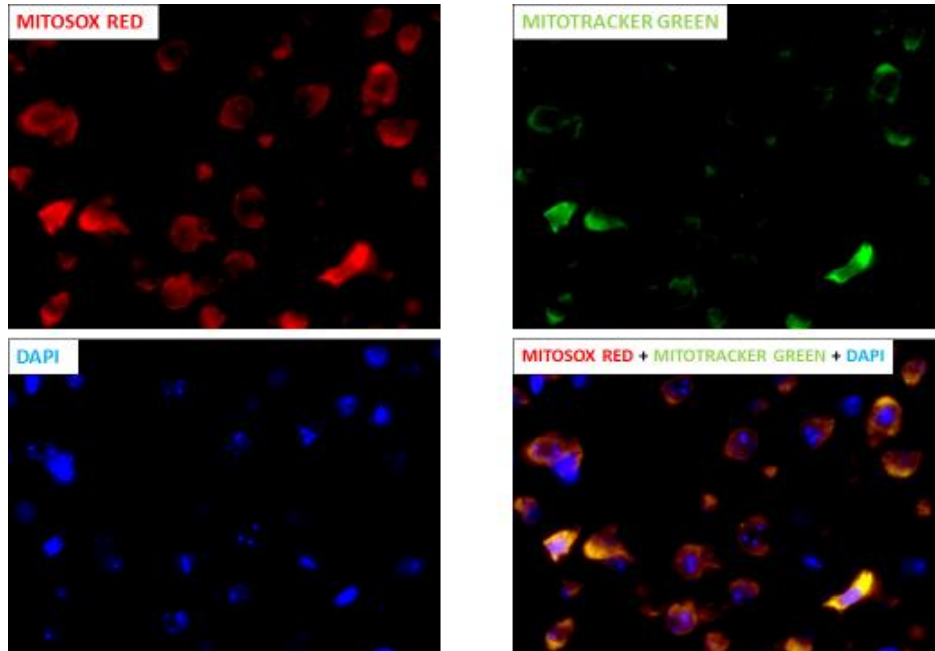
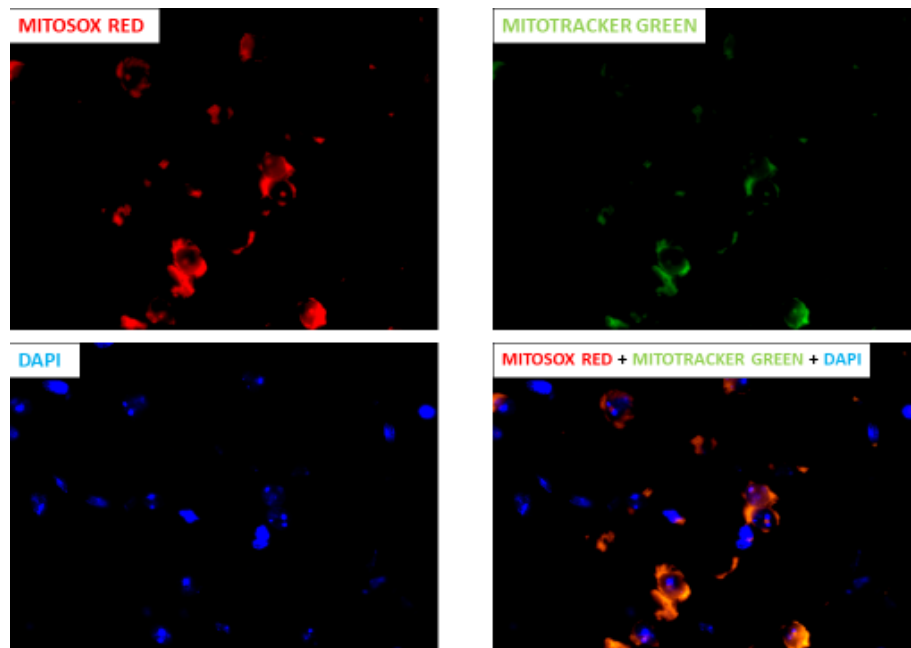


Figure 14

A

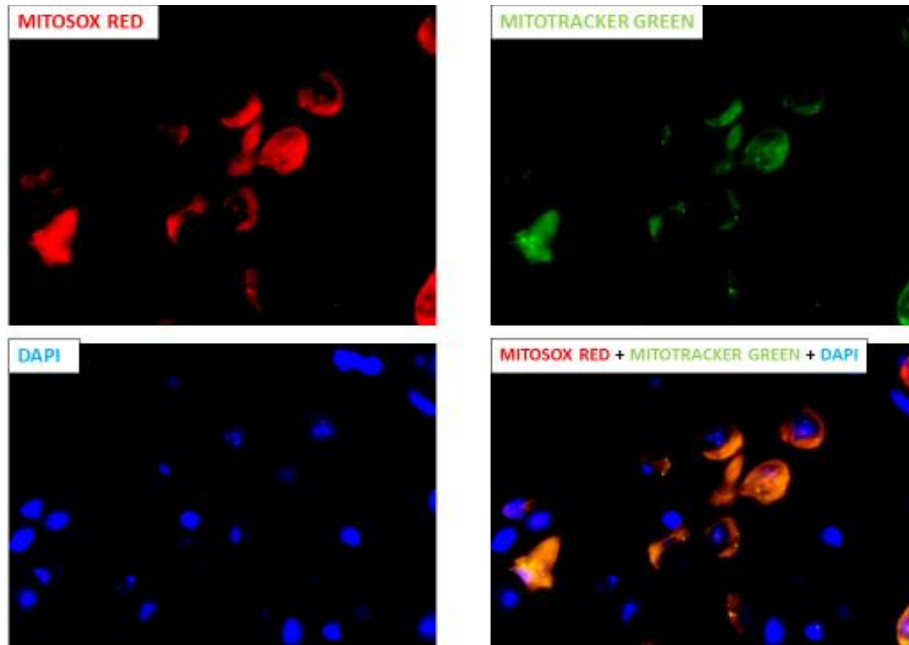


RNP PERI-INFARCTED AREA

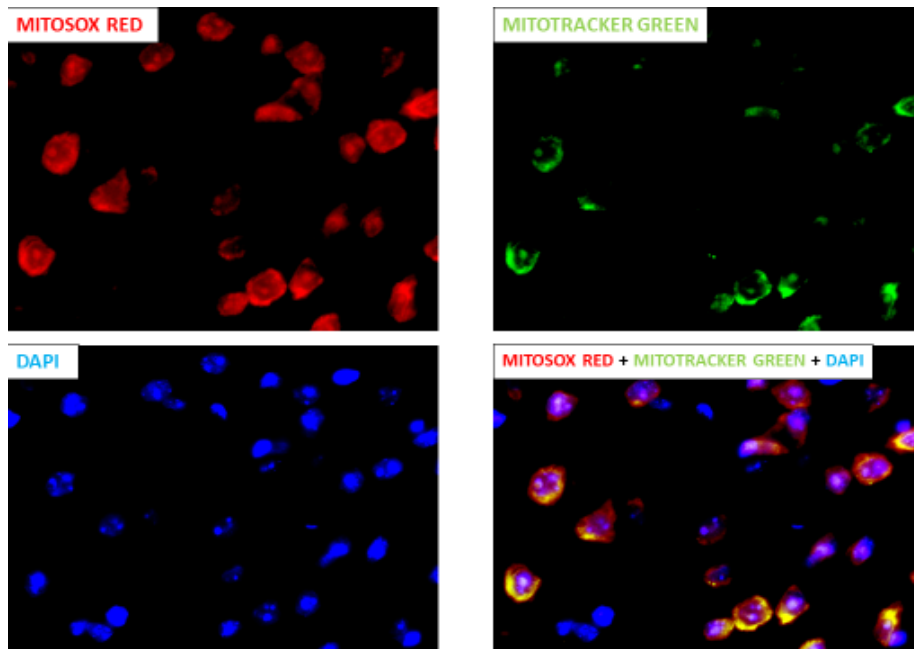


RNP CORE OF THE INFARCTED AREA

B

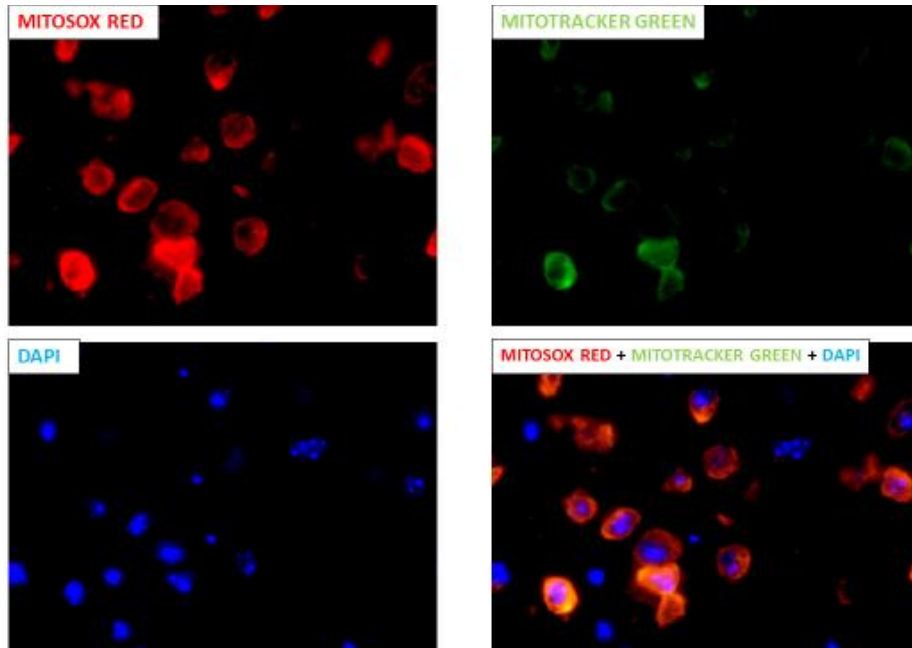


EDARAVONE PERI-INFARCTED AREA

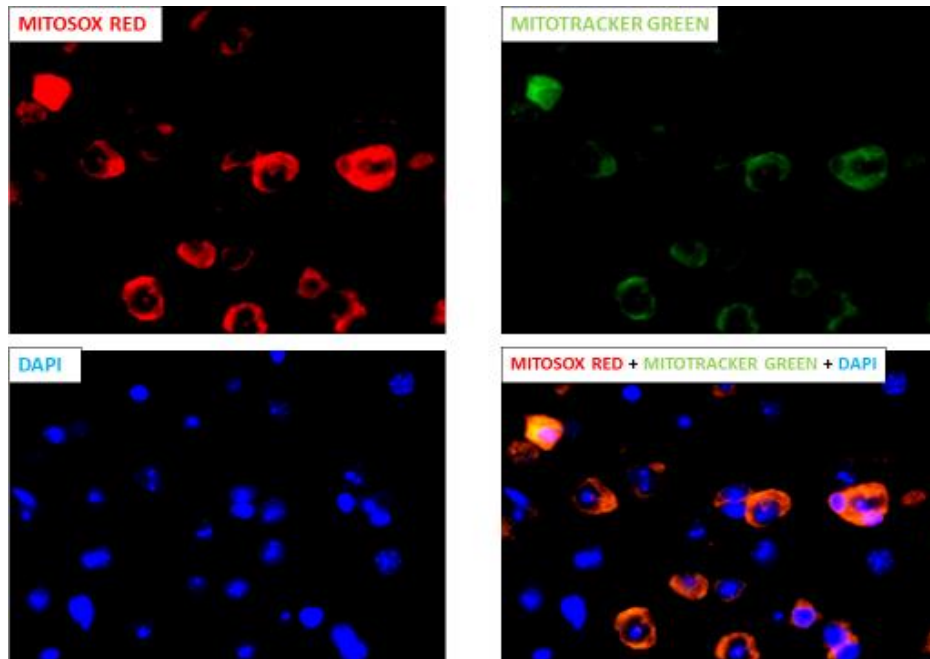


EDARAVONE CORE OF THE INFARCTED AREA

C

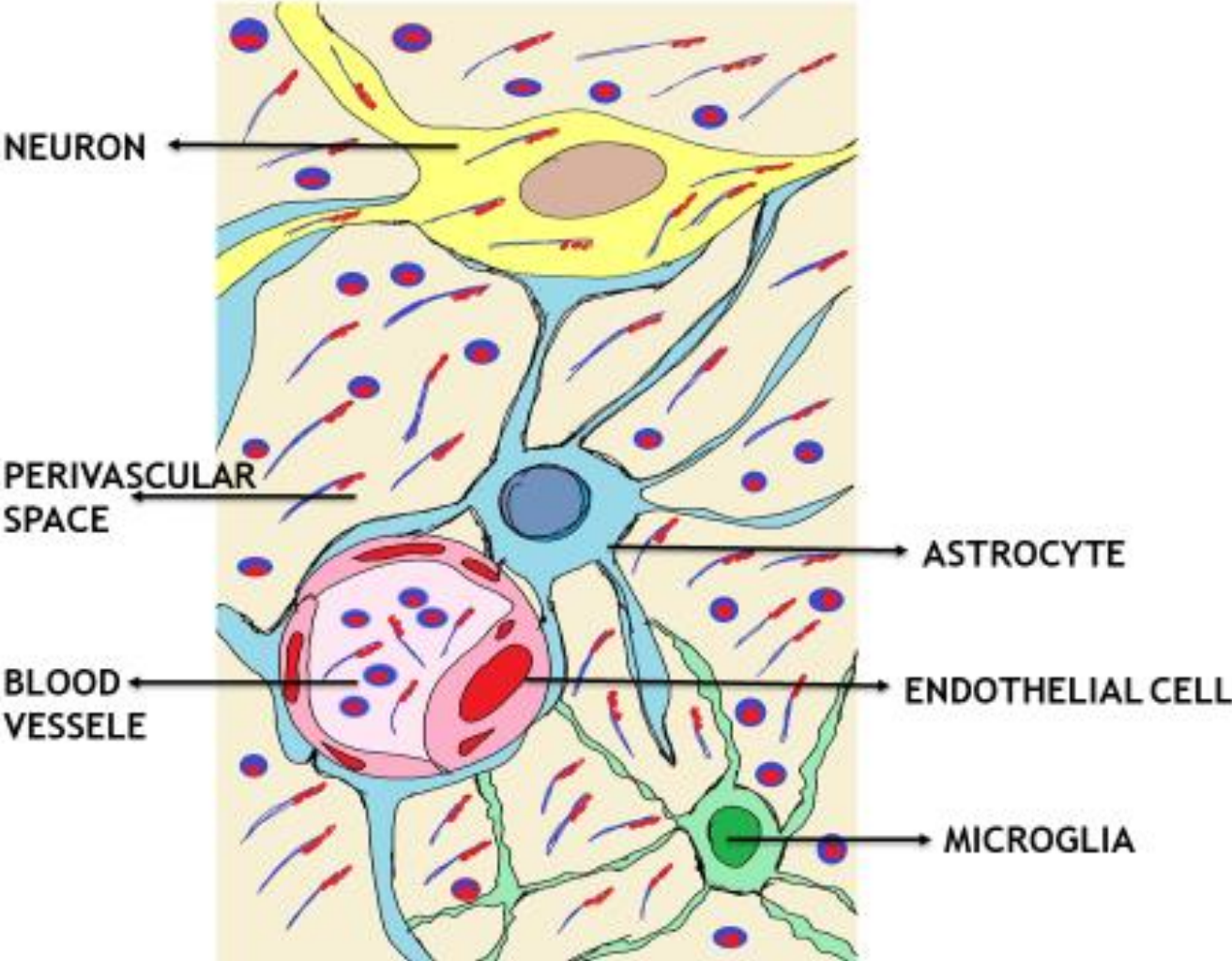




PBS PERI-INFARTCED AREA



PBS CORE OF THE INFARCTED AREA

Figure 15



-  RNP
-  Polymer

CHAPTER 9 REFERENCES

1. Broderick JP, Berkhemer OA, Palesch YY, et al. Endovascular therapy is effective and safe for patients with severe ischemic stroke: Pooled analysis of interventional management of stroke III and multicenter randomized clinical trial of endovascular therapy for acute ischemic stroke in the netherlands data. *Stroke*. 2015; 46: 3416-3422.
2. Campbell BC, Mitchell PJ, Kleinig TJ, et al. Endovascular therapy for ischemic stroke with perfusion-imaging selection. *N Engl J Med*. 2015; 372: 1009-1018.
3. Goyal M, Demchuk AM, Menon BK, et al. Randomized assessment of rapid endovascular treatment of ischemic stroke. *N Engl J Med*. 2015; 372: 1019-1030.
4. Feigin VL, Norrving B, and Mensah GA. Global burden of stroke. *Circ Res*. 2017; 120: 439-448.
5. Grech R, Schembri M, Thornton J. Stent-based thrombectomy versus intravenous tissue plasminogen activator in acute ischaemic stroke: A systematic review and meta-analysis. *Interv Neuroradiol*. 2015; 21: 684-690.
6. Lambrinos A, Schaink AK, Dhalla I, et al. Mechanical Thrombectomy in Acute Ischemic Stroke: A Systematic Review. *Can J Neurol Sci*. 2016; 43:455-460.
7. Jovin TG, Chamorro A, Cobo E, et al. Thrombectomy within 8 hours after symptom onset in ischemic stroke. *N Engl J Med*. 2015; 372: 2296-2306.
8. Evans MRB, White P, Cowley P, Werring DJ. Revolution in acute ischaemic stroke care: a practical guide to mechanical thrombectomy. *Pract Neurol*. 2017; 17: 252-265.
9. Rodrigues, Filipe Brogueira et al. Endovascular treatment versus medical care alone for ischaemic stroke: systematic review and meta-analysis. *BMJ (Clinical research ed.)* vol. 353 i1754.

10. Egashira Y, Yoshimura S, Sakai N, Kuwayama N. Efficacy of endovascular revascularization in elderly patients with acute large vessel occlusion: Analysis from RESCUE-Japan retrospective nationwide survey. *J Stroke Cerebrovasc Dis.* 2013; 22: 627-632.
11. Soule BP, Hyodo F, Matsumoto K, et al. The chemistry and biology of nitroxide compounds. *Free Radic Biol Med.* 2007; 42: 1632-1650.
12. Kato N, Yanaka K, Hyodo K, et al. Stable nitroxide tempol ameliorates brain injury by inhibiting lipid peroxidation in a rat model of transient focal cerebral ischemia. *Brain Research.* 2003; 979: 188-193.
13. Rak R, Chao DL, Pluta RM, et al. Neuroprotection by the stable nitroxide tempol during reperfusion in a rat model of transient focal ischemia. *J Neurosurg.* 2000; 92: 646–651.
14. Hahn SM, Sullivan FJ, DeLuca AM, et al. Hemodynamic effect of the nitroxide superoxide dismutase mimics. *Free Radic Biol Med.* 1999; 27: 529-535.
15. Hosoo H, Marushima A, Nagasaki Y, et al. Neurovascular unit protection from cerebral ischemia–reperfusion injury by radical-containing nanoparticles in mice. *Stroke.* 2017; 48: 2238-2247.
16. Marushima A, Suzuki K, Nagasaki Y, et al. Newly synthesized radical-containing nanoparticles enhance neuroprotection after cerebral ischemia-reperfusion injury. *Neurosurgery.* 2011; 68: 1418-1426.
17. Mei T, Kim A, Vong LB, et al. Encapsulation of tissue plasminogen activator in pH-sensitive self-assembled antioxidant nanoparticles for ischemic stroke treatment - Synergistic effect of thrombolysis and antioxidant. *Biomaterials.* 2019; 215: 119209.
18. Lapchak P, A Critical Assessment of Edaravone Acute Stroke Efficacy Trials: Is a Edaravone an Effective Neuroprotective Therapy? *Expert Opin Pharmacother.* 2010; 11: 1753-1763.

19. Watanabe T, Tahara M, Todo S. The novel antioxidant edaravone: from bench to bedside. *Cardiovasc Ther.* 2008; 26: 101-114.
20. Yoshida H, Yanai H, Namiki Y, Fukatsu-Sasaki K, Furutani N, Tada N. Neuroprotective effects of edaravone: a novel free radical scavenger in cerebrovascular injury. *CNS Drug Rev.* 2006; 12: 9-20.
21. Lee BJ, Egi Y, van Leyen K, Lo EH, Arai K. Edaravone, a free radical scavenger, protects components of the neurovascular unit against oxidative stress in vitro. *Brain Res.* 2010 11; 1307: 22-27.
22. Higashi Y. Edaravone for the treatment of acute cerebral infarction: role of endothelium-derived nitric oxide and oxidative stress. *Expert Opin Pharmacother.* 2009; 10: 323-331.
23. Yoshitomi T, Suzuki R, Mamiya T, et al. pH-sensitive radical-containing-nanoparticle (RNP) for the I-band-epr imaging of low pH circumstances. *Bioconjug Chem.* 2009; 20: 1792-1798.
24. Yoshitomi T, Miyamoto D, and Nagasaki Y. Design of core-shell-type nanoparticles carrying stable radicals in the core. *Biomacromolecules.* 2009; 10: 596-601.
25. Ansari S, Azari H, McConnell DJ, et al. Intraluminal middle cerebral artery occlusion (mcao) model for ischemic stroke with laser doppler flowmetry guidance in mice. *J Vis Exp.* 2011; 51: e2879.
26. Yarnell, A.M., Barry, E.S., Mountney, A., Shear, D., Tortella, F., and Grunberg, N.E. 2016. The revised neurobehavioral severity scale (NSS-R) for rodents. *Curr. Protoc. Neurosci.* 2016 ; 75: 9.52.1-9.52.16.
27. Balkaya M, Krober JM et al. Assessing post-stroke behavior in mouse models of focal ischemia, *Journal of Cerebral Blood Flow & Metabolism.* 2013; 33: 330-338.

28. Takahashi T et al. Novel neuroprotection using antioxidant nanoparticles in a mouse model of head trauma, *Journal of Trauma and Acute Care Surgery*. 2020; 88: 677-685.
29. Manaenko A, Chen H, Kammer J, et al. Comparison evans blue injection routes: Intravenous versus intraperitoneal, for measurement of blood-brain barrier in a mice hemorrhage model. *J Neurosci Methods*. 2011; 195: 206-210.
30. Devraj K, Guérit S, Macas J, Reiss Y. An In Vivo Blood-brain Barrier Permeability Assay in Mice Using Fluorescently Labeled Tracers. *J Vis Exp*. 2018; 132: 57038.
31. Rakos G, Kis Z, Nagy D, et al. Evans Blue fluorescence permits the rapid visualization of non-intact cells in the perilesional rim od cold-injured rat brain. *Acta Neurobiol Exp*. 2007; 67; 149-154.
32. Oowada S, Endo N, Kameya H, et al. Multiple free-radical scavenging capacity in serum. *J Clin Biochem Nutr*. 2012; 51: 117-121.
33. Furumoto K, Nagayama S, Ogawara K, et al. Hepatic uptake of negatively charged particles in rats: Possible involvement of serum proteins in recognition by scavenger receptor. *J Control Release*. 2004; 97: 133-141.
34. Khan AR, Yang X, Fu M, et al. Recent progress of drug nanoformulations targeting to brain. *J Control Release*. 2018; 291: 37-64.
35. Hu X, Li P, Guo Y, et al. Microglia/macrophage polarization dynamics reveal novel mechanism of injury expansion after focal cerebral ischemia. *Stroke*. 2012; 43: 3063-3070.
36. Wang G, Zhang J, Hu X, et al. Microglia/macrophage polarization dynamics in white matter after traumatic brain injury. *J Cereb Blood Flow Metab*. 2013; 33: 1864-1874.

37. Barakat R and Redzic Z. The role of activated microglia and resident macrophages in the neurovascular unit during cerebral ischemia: is the jury still out? *Med Princ Pract.* 2016; 25 Suppl 1: 3-14.
38. Vosler PS, Graham SH, Wechsler LR, Chen J, Mitochondrial targets for stroke: focusing basic science research toward development of clinically translatable therapeutics. *Stroke.* 2009; 40: 3149-3155.
39. Huang JI, Manaenko A, Ye ZH, Sun XY, Hu Q, Hypoxia therapy- a new hope for the treatment of mitochondrial dysfunctions. *Med. Gas Res.* 2016; 6 : 174.
40. Kunz A, Park L, Abe T, Gallo EF, Anrather J, Zhou P, Iadecola C. Neurovascular protection by ischemic tolerance: role of nitric oxide and reactive oxygen species. *J. Neurosci.* 2007; 27 : 7083-7093.
41. Lin MT, Beal MF. Mitochondrial dysfunction and oxidative stress in neurodegenerative diseases. *Nature.* 2006; 443: 787.
42. Sims NR, Muyderman H. Mitochondria, oxidative metabolism and cell death in stroke. *Biochim. Biophys. Acta (BBA) - Mol. Basis Dis.* 2010; 1802: 80-91.
43. Sanderson TH, Reynolds CA, Kumar R, Przyklenk K, Hutteman M. Molecular mechanisms of ischemia–reperfusion injury in brain: pivotal role of the mitochondrial membrane potential in reactive oxygen species generation. *Mol. Neurobiol.* 2013; 47: 9-23.
44. Liu F, McCullough LD, Middle Cerebral Artery Occlusion Model in Rodents: Methods and Potential Pitfalls. *J Biomed Biotechnol.* 2011; 464701.
45. Liu F, Yuan R, Benashski SE, McCullough LD. Changes in experimental stroke outcome across the life span. *Journal of Cerebral Blood Flow and Metabolism.* 2009; 29: 792-802.

CHAPTER 10 SOURCE

The contents previously published in Brain Research Volume 1743, 15 September, 146922; Mujagić A, Marushima A, Nagasaki Y, Hosoo H, Hirayama A, Puentes S, Takahashi T, Tsurushima H, Suzuki K, Matsui H, Ishikawa E, Matsumaru Y, Matsumura A; Antioxidant nanomedicine with cytoplasmic distribution in neuronal cells shows superior neurovascular protection properties; Copyright Elsevier (2020); are re-used in this dissertation based on the approval from Elsevier B.V.

Following is the link to the final published version hosted on the Science Direct;
<https://doi.org/10.1016/j.brainres.2020.146922>.

CHAPTER 11 ACKNOWLEDGMENTS

For his never-failing support and guidance, I would like to express my deepest gratitude to Professor Akira Matsumura from Department of Neurosurgery, University of Tsukuba.

I would like to thank Professor Yuji Matsumaru for his valuable guidance and support.

In addition, I would like to thank Assistant Professor Aiki Marushima. It is because of his bright example of what true scholar and surgeon is and thanks to his direct guidance in all the phases of research presented here, that I was able to accomplish my goal of writing this thesis.

I would like to express my gratitude to Professor Yukio Nagasaki from Graduate School of Pure and Applied Sciences, University of Tsukuba who created RNPs and provided it free of charge, and helped me with his guidance on research method and thesis writing. I am thankful to Professor Akira Hirayama from Center for Integrative Medicine, Tsukuba University of Technology for his guidance in evaluation of ROS scavenging capacities.

I would like to thank Ms. Yoshiko Tsukada and Ms. Makiko Miyakawa from Graduate School of Comprehensive Human Sciences, University of Tsukuba, for their unfailing technical support, time and effort they have most generously invested in this study. I would also like to express my gratitude to Dr. Yumiko Nagano from Center for Integrative Medicine, Tsukuba University of Technology, for the effort and time, she most kindly invested, in measurement and analysis of multiple free radical-scavenging capacities using electron paramagnetic resonance-based method.

参 考 论 文